


SUPPLEMENTAL GROUNDWATER MODELING REPORT FOR THE SPLIT ROCK, WYOMING SITE

Prepared For:

**NUCLEAR REGULATORY COMMISSION
11545 Rockville Pike
Rockville, Maryland 20852**

Prepared By:




consulting
scientists and
engineers

**3801 Automation Way, Suite 100
Fort Collins, Colorado 80525**

March 2003

SUPPLEMENTAL GROUNDWATER MODELING REPORT FOR THE SPLIT ROCK, WYOMING SITE

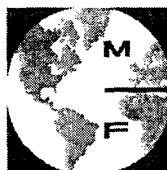
Prepared For:

Nuclear Regulatory Commission
11545 Rockville Pike
Rockville, Maryland 20852

Prepared By:

MFG, Inc.
3801 Automation Way, Suite 100
Fort Collins, Colorado 80525

March 2003



G
consulting
scientists and
engineers

TABLE OF CONTENTS

1.0	INTRODUCTION.....	1
2.0	BACKGROUND.....	3
2.1	Site History.....	3
2.2	Conceptual Model.....	3
3.0	MODEL DEVELOPMENT.....	5
3.1	Overview.....	5
3.2	Groundwater Vistas.....	6
3.3	Groundwater Flow Model.....	6
3.4	Solute Transport Model.....	6
3.5	PEST.....	6
3.6	Model Domain.....	7
4.0	FLOW CALIBRATION.....	8
4.1	Head Targets.....	8
4.2	Well Pumping and Stress Periods.....	8
4.3	Precipitation Recharge.....	9
4.4	Impoundment Recharge.....	10
4.5	Specific Yield.....	11
4.6	Calibrated Hydraulic Conductivity.....	11
5.0	TRANSPORT CALIBRATION.....	13
5.1	Transport Targets.....	13
5.2	Prescribed Source Zone.....	13
5.3	Initial Concentrations.....	15
5.4	Effective Porosity and Dispersion.....	16
5.5	Retardation of Uranium and K_d	17
6.0	PREDICTIVE TRANSPORT MODEL RESULTS.....	19
7.0	REFERENCES.....	20

LIST OF ATTACHMENTS

Attachment A Sensitivity Analysis

LIST OF TABLES

Table 4.1-1	Calibration Head Targets
Table 4.2-1	Well Pumping and Stress Period Designation
Table 4.3-1	Jeffrey City Monthly Precipitation Record
Table 4.3-2	Precipitation Recharge Adjustment Ratio
Table 5.1-1	Concentration Target Wells
Table 5.3-1	Initial Concentration Plume Wells

LIST OF FIGURES

- Figure 3.6-1 Model domain and grid
- Figure 4.1-1 Head target well locations
- Figure 4.3-1 Model recharge zones
- Figure 4.4-1 Impoundment seepage recharge estimate
- Figure 4.5-1 Hydraulic conductivity zone boundaries, Layer 1
- Figure 4.5-2 Hydraulic conductivity zone boundaries, Layer 2
- Figure 4.5-3 Hydraulic conductivity zone boundaries, Layer 3
- Figure 4.5-4 Specific yield/porosity zone boundaries
- Figure 4.6-1 Calibrated hydraulic conductivity, southwest valley region
- Figure 4.6-2 WELL-1 Observed vs. Simulated Ground Water Hydrograph
- Figure 4.6-3 WELL-3 Observed vs. Simulated Ground Water Hydrograph
- Figure 4.6-4 WN-15 Observed vs. Simulated Ground Water Hydrograph
- Figure 4.6-5 WN-21 Observed vs. Simulated Ground Water Hydrograph
- Figure 4.6-6 WN-24 Observed vs. Simulated Ground Water Hydrograph
- Figure 4.6-7 WN-25 Observed vs. Simulated Ground Water Hydrograph
- Figure 4.6-8 WN-16 Observed vs. Simulated Ground Water Hydrograph
- Figure 4.6-9 WN-A Observed vs. Simulated Ground Water Hydrograph
- Figure 4.6-10 WN-B Observed vs. Simulated Ground Water Hydrograph
- Figure 4.6-11 WN-C Observed vs. Simulated Ground Water Hydrograph
- Figure 4.6-12 WELL-6 Observed vs. Simulated Ground Water Hydrograph
- Figure 4.6-13 WN-11 Observed vs. Simulated Ground Water Hydrograph
- Figure 4.6-14 WELL-4 Observed vs. Simulated Ground Water Hydrograph
- Figure 4.6-15 WELL-5 Observed vs. Simulated Ground Water Hydrograph
- Figure 4.6-16 WN-17 Observed vs. Simulated Ground Water Hydrograph
- Figure 4.6-17 WN-18 Observed vs. Simulated Ground Water Hydrograph
- Figure 4.6-18 SWAB-14 Observed vs. Simulated Ground Water Hydrograph
- Figure 4.6-19 SAB-8 Observed vs. Simulated Ground Water Hydrograph
- Figure 4.6-20 SWAB-6 Observed vs. Simulated Ground Water Hydrograph
- Figure 4.6-21 SAB-3 Observed vs. Simulated Ground Water Hydrograph
- Figure 4.6-22 SWAB-33 Observed vs. Simulated Ground Water Hydrograph
- Figure 4.6-23 SWAB-31 Observed vs. Simulated Ground Water Hydrograph
- Figure 4.6-24 SWAB-34 Observed vs. Simulated Ground Water Hydrograph
- Figure 4.6-25 SWAB-32 Observed vs. Simulated Ground Water Hydrograph
- Figure 4.6-26 SWAB-29 Observed vs. Simulated Ground Water Hydrograph
- Figure 5.1-1 Concentration target well locations
- Figure 5.2-1 Site model domain showing prescribed source zone
- Figure 5.2-2 Prescribed uranium source zone cross section
- Figure 5.2-3 Prescribed sulfate source zone cross section
- Figure 5.3-1 Calibrated layer 1 initial sulfate concentrations (mg/L)
- Figure 5.3-2 Calibrated layer 2 initial sulfate concentrations (mg/L)
- Figure 5.3-3 Calibrated layer 1 initial uranium concentrations (mg/L)
- Figure 5.3-4 Calibrated layer 2 initial uranium concentrations (mg/L)
- Figure 5.3-5 Predictive simulation layer 1 initial sulfate concentrations (mg/L)
- Figure 5.3-6 Predictive simulation layer 2 initial sulfate concentrations (mg/L)
- Figure 5.3-7 Predictive simulation layer 1 initial uranium concentrations (mg/L)
- Figure 5.3-8 Predictive simulation layer 2 initial uranium concentrations (mg/L)

Figure 5.4-1	SWAB-1 Simulated vs. observed sulfate chemograph
Figure 5.4-2	SWAB-10 Simulated vs. observed sulfate chemograph
Figure 5.4-3	SWAB-11 Simulated vs. observed sulfate chemograph
Figure 5.4-4	SWAB-15 Simulated vs. observed sulfate chemograph
Figure 5.4-5	SWAB-3 Simulated vs. observed sulfate chemograph
Figure 5.4-6	SWAB-7 Simulated vs. observed sulfate chemograph
Figure 5.4-7	SWAB-8 Simulated vs. observed sulfate chemograph
Figure 5.4-8	SWEB-11 Simulated vs. observed sulfate chemograph
Figure 5.4-9	SWEB-12 Simulated vs. observed sulfate chemograph
Figure 5.4-10	SWEB-6 Simulated vs. observed sulfate chemograph
Figure 5.4-11	SWEB-8 Simulated vs. observed sulfate chemograph
Figure 5.4-12	WELL-3 Simulated vs. observed sulfate chemograph
Figure 5.4-13	WN-15 Simulated vs. observed sulfate chemograph
Figure 5.4-14	WN-21 Simulated vs. observed sulfate chemograph
Figure 5.4-15	WN-24 Simulated vs. observed sulfate chemograph
Figure 5.4-16	WN-25 Simulated vs. observed sulfate chemograph
Figure 5.5-1	WN-B Sulfate vs. uranium transport comparison
Figure 5.5-2	WN-C Sulfate vs. uranium transport comparison
Figure 5.5-3	WELL-3 Sulfate vs. uranium transport comparison
Figure 5.5-4	WN-21 Sulfate vs. uranium transport comparison
Figure 5.5-5	WN-24 Sulfate vs. uranium transport comparison
Figure 5.5-6	WN-25 Sulfate vs. uranium transport comparison
Figure 5.5-7	WN-15 Sulfate vs. uranium transport comparison
Figure 5.5-8	SWAB-1 Simulated vs. observed uranium chemograph
Figure 5.5-9	SWAB-11 Simulated vs. observed uranium chemograph
Figure 5.5-10	SWAB-15 Simulated vs. observed uranium chemograph
Figure 5.5-11	SWAB-3 Simulated vs. observed uranium chemograph
Figure 5.5-12	SWAB-7 Simulated vs. observed uranium chemograph
Figure 5.5-13	SWAB-8 Simulated vs. observed uranium chemograph
Figure 5.5-14	SWEB-11 Simulated vs. observed uranium chemograph
Figure 5.5-15	SWEB-12 Simulated vs. observed uranium chemograph
Figure 5.5-16	SWEB-6 Simulated vs. observed uranium chemograph
Figure 5.5-17	SWEB-8 Simulated vs. observed uranium chemograph
Figure 5.5-18	WELL-3 Simulated vs. observed uranium chemograph
Figure 5.5-19	WN-15 Simulated vs. observed uranium chemograph
Figure 5.5-20	WN-21 Simulated vs. observed uranium chemograph
Figure 5.5-21	WN-24 Simulated vs. observed uranium chemograph
Figure 5.5-22	WN-25 Simulated vs. observed uranium chemograph
Figure 6.0-1	Predicted 200 year sulfate concentrations mg/L
Figure 6.0-2	Predicted 500 year sulfate concentrations mg/L
Figure 6.0-3	Predicted 1000 year sulfate concentrations mg/L
Figure 6.0-4	Predicted 200 year uranium concentrations mg/L
Figure 6.0-5	Predicted 500 year uranium concentrations mg/L
Figure 6.0-6	Predicted 1000 year uranium concentrations mg/L
Figure 6.0-7	Proposed long-term care boundary with predicted 1000 year uranium plume

1.0 INTRODUCTION

This report describes a thorough revision of the numerical groundwater flow and solute transport models previously developed in connection with the 1999 Groundwater Protection Plan (GWPP) for the Split Rock Mill Site (SMI, 1999). The reason for revising the models has been to improve confidence in the predictions of COC migration beyond the Southwest Valley. New sampling data, collected through the on-going monitoring of both previously existing and newly installed wells have increased the understanding of trends toward long-term conditions, and has been used to guide the modeling process. New modeling codes and the advent of inverse modeling methods have, in part, made this exercise possible. Many of the techniques used in the calibration of this model were not available at the time the original model was completed. The elimination of certain simplifying assumptions employed in the previous steady-state models have produced transient simulations that more closely match observed site behavior. It is reasonable to expect that given the improvements in calibrated model accuracy, the predictive simulations are also improved and increased confidence can be placed in future predictions.

The data used to calibrate the previous flow and transport models extended only through 1996. The revised model incorporates an additional 6 years of quarterly sampling data gathered since that time as part of the Corrective Action Program (CAP). This time period has been marked by greatly reduced hydraulic stresses from the CAP pumping wells. Trends have been revealed which could only have been conjectured from the snapshot of information obtained for wells installed in 1996. It is precisely these trends that factor so heavily in the understanding of site hydro-dynamics, and which lead to the accurate prediction of long-term conditions.

In addition to extending the calibration period, the start of the calibration period was moved backward in time to allow the inclusion of more target piezometric and analytical data with which to compare simulated model output. Frequent site-wide monitoring of water levels and analytical measurement of dissolved constituents from 1981 onward provides ample data resolution to support comparisons of observed and simulated parameters. The availability of more comparisons allows increased refinement of model parameters to match model behavior to site behavior.

The changing flux from the tailings pond, and changes in well pumping from both the facility and Jeffery City water supply have resulted in pronounced changes in hydraulic gradient through the Southwest Valley and surroundings. The assumption of steady state flow for calibration and prediction in the previous flow models was made to simplify the calibration process, but failed to capture the changing

hydraulic gradients that drive solute transport. The basic definition of a steady state flow system is one in which inputs equal outputs and there is no change in storage within the system. Inspection of the site history reveals that water storage in the impoundment area and the underlying aquifer went through a period of substantial increase, followed by a period of significant drainage. The steady state flow approximation has been replaced by an inherently more accurate transient solution technique. The approach to steady state conditions is not expected to occur for many years to come. For this reason, the predictive simulations also share the transient scheme. A better representation of site hydrology by the model is afforded by this change to transient flow.

The assumption that dissolved uranium is transported without retardation is considered to be highly conservative. A more realistic approach has now been applied, in which the retardation of uranium transport is included in model calibration and subsequent predictions. The coexistence of both uranium and sulfate sampling data for the Split Rock Mill Site provides a means to calibrate the transport model for both sulfate (chemically conservative) and uranium (retarded). Because of closer agreement between simulated and observed solute transport over the calibration period, predictions of COC migration are now considered more representative than in the previous model.

The remainder of this report has been divided into six sections, plus two attachments. The next section (2) helps to place this modeling supplement into the broader framework of the activities related to closure of the Split Rock Mill Site. A model development section to introduce the overall scope and method of the modeling effort follows this. Section four and five contain the specific details of the model revision for the flow and transport phases of the model, respectively. The model predictions of contaminant migration are presented in section six. References are in section seven. There is also an attached sensitivity analysis (A.1) that supports the model conclusions, but has been kept separate from the report body because of its requisite level of technical intricacy. Finally, the computer files that constitute the numerical models are provided on the attached Compact Disc.

2.0 BACKGROUND

The comprehensive GWPP submitted to the NRC by Western Nuclear Inc. (SMI, 1999) included numerical groundwater flow and solute transport models. The models provide a means for understanding the historic and current groundwater flow regime and serve as a tool for simulating the migration of dissolved constituents beyond the reclaimed site area. The development of those models relied upon the detailed characterization of the hydrologic, geologic and geochemical properties of the mill site and surroundings that is also contained in the GWPP.

Although the current report contains model developments that are intended to supersede those in the previous submittal, there remains a vital dependence upon the established rigorous characterization. Portions of the GWPP that are especially relevant to this report include the Site History, and the Hydrogeologic Conceptual Model. The remainder of this section outlines the key elements of these articles, and gives reference to more detailed discussion in the GWPP.

2.1 Site History

In order to better understand how the time period simulated in the model relates to events that took place at the site, the history of the site can be divided into four operational time periods:

- Main Operational and Early Standby Period (1957 to 1983)
- Period of Pump back to Control Valley Seepage (1983 to 1986)
- Period of Main Tailing Pond Drainage (1986 to 1989)
- Period of Corrective Action Program Well Pumping and Reclamation (1990 to present)

Each change of period marks a transition of major hydrologic stresses. A detailed description of the Site History is contained in Section E.2 of the GWPP (SMI, 1999).

2.2 Conceptual Model

The conceptual model serves as the foundation for the numerical models. Because little has changed with regard to conceptual understanding of the Split Rock Site from the GWPP, many aspects of the previous numerical models have been duplicated in the current numerical models. Important elements of the conceptual model include the following:

- Hydrostratigraphic Units (HSUs)

- Regional Groundwater Flow
- Local Groundwater Flow
- Surface Water/Groundwater Interaction
- Recharge/Evapotranspiration
- Discharge to the Sweetwater River
- Pumping Stresses
- Water Budget.

Detailed discussions of these features can be found in Appendix E.3 of the GWPP (SMI, 1999).

3.0 MODEL DEVELOPMENT

This section provides a general discussion on the steps that were taken and the tools used to create the revised model. There are numerous references to text and figures in the GWPP (SMI, 1999). More specific details on each step of the process are discussed in the following sections of the report.

3.1 Overview

An overview of the modeling process helps to give context to the particular details presented in the remainder of this section. This numerical groundwater flow modeling process has a calibration phase and a prediction phase. The solute transport modeling also shares these two phases, and relies heavily upon the results of the flow models as input. The hierarchy relating the various model phases has important implications toward the order in which they are addressed.

The flow calibration phase is primary. Aspects of the site that are suspected of contributing to groundwater occurrence and movement are represented in the model. Parameters that are known with a high degree of confidence are typically left unchanged, while those that are not become the focus of calibration. Recorded hydraulic head measurements are used as targets to directly compare with model simulated heads in order to judge the accuracy of the simulation. Refinements are then made to the model parameters within accepted ranges to minimize discrepancies.

The transport model calculates the solute movement through the aquifer based on the modeled flow and the values assigned to various transport parameters. Transport calibration includes the development of an existing plume at the initial time and the source term used to simulate continuing contaminant loading. Some transport parameters are associated with the aquifer properties, while others are solute specific. Constituent concentration targets are derived from analytical measurement of groundwater sampling and serve to guide the calibration of transport parameters in a similar manner to flow calibration; Transport parameters are modified until modeled output closely matches the analytical data.

The flow prediction phase relies upon the optimized flow model parameters of the calibration phase, and uses forecast stresses to anticipate future groundwater levels and movement. The time simulated in the prediction phase begins at the end of the calibration phase, and runs up through the future time of interest. Analogous to the dependence of transport to flow models during calibration, the predictive transport simulation requires the predicted flow model's velocities. Solute migration is then calculated using the calibrated transport parameters.

3.2 Groundwater Vistas

The models presented in this report have been constructed using Groundwater Vistas version 3.38 (Rumbaugh and Rumbaugh, 2001) licensed by Environmental Simulations, Inc. Groundwater Vistas is a pre- and post- processing modeling environment for Microsoft Windows that couples a model design system with comprehensive graphical analysis tools. This program provides visualization of model development and results, and allows for enhanced model quality and accuracy. Although Groundwater Vistas supports a wide variety of flow and transport models it was used in this project for the development of MODFLOW-2000 and MT3DMS modeling files and for processing modeling results.

3.3 Groundwater Flow Model

The model code used in this project for flow simulation is MODFLOW-2000. This is a public domain, three-dimensional finite difference flow model developed by Harbaugh and others (2000) for the U.S. Geological Survey (USGS). Among its enhancements over previous versions of MODFLOW is the capability to simulate both steady state and transient stress periods within a single model run. This feature can be useful in establishing the initial heads for the model during the first stress period, while preserving the transient character in all subsequent stress periods. Another improvement is that leakance between model layers is calculated for each time step based on the difference in hydraulic head of the layers, instead of remaining a fixed value calculated only at the start of the simulation. This improves the accuracy of flow between layers if there are significant changes in water levels during the simulation.

3.4 Solute Transport Model

The model code used to simulate solute transport for this project is MT3DMS. This is a public domain, three-dimensional multi-species transport code originally written by Zheng and Wang (1999) under contract to the U.S. Environmental Protection Agency (EPA) and later modified for the U.S. Army Core Of Engineers (COE). The code has been extensively tested, and is widely used and accepted. MT3DMS has comprehensive capabilities for simulating advection, dispersion and chemical reactions, including retardation, of dissolved constituents in groundwater flow systems.

3.5 PEST

PEST™ is a nonlinear parameter estimation package (Doherty, 1999). PEST can directly interface with Groundwater Vistas, allowing automated calibration of a groundwater model with observed conditions. PEST can be used to estimate parameters for just about any existing computer model, such as

MODFLOW, MT3DMS, RT3D, SEAM3D, and FEMWATER. PEST is able to “take control” of a model, running it as many times as required while adjusting model parameters until the discrepancies between selected model outputs and a complementary set of field or laboratory measurements are reduced to an acceptable statistical minimum. Pest was used during the calibration of both the flow and transport calibration simulations.

3.6 Model Domain

The development of the model grid and layers in the original model (Appendix E.4; SMI, 1999) was deemed appropriate for the new models, and has been reproduced for the current models. The one improvement made to the model domain was to start the modeling process using the expanded grid that had been previously adapted only for long-term predictive runs in order to provide sufficient lateral extent to encompass long-term plume migration (Figure 3.6-1). The active model area is bounded on the north by the Sweetwater River (a head-dependant flux boundary) and on the south by a streamline (i.e., no-flow) boundary. Western and eastern boundaries are represented as prescribed head boundaries. The eastern, western, and southern boundaries are set at sufficient distances that modeled responses at the site are not affected by those boundary conditions. Thus the model domain is “seemingly” infinite in the eastern, western, and southern directions.

The domain is a rectangle, with the north to south dimension approximately 34,000 feet in length, and an east to west dimension of approximately 60,000 feet. The model grid consists of 106 rows by 264 columns by 3 layers representing the distinct HSUs. The northeast portion of the model domain is grid with uniform 200x200 foot cells. This area includes Jeffrey City, the Split Rock Mill Site, and all areas to the east the granite outcrops.

4.0 FLOW CALIBRATION

The time simulated by the calibration phase is chosen to include all the relevant recorded groundwater levels and well pumping rates. The calibration time period starts in 1981 and ends in 2002, which is the maximum time span coincident with sufficient recorded hydrologic and geochemical data available for comparison. Boundary conditions are set up in the model to emulate the geometry of features such as rivers, and impermeable barriers to flow. Inflows to and outflows from the aquifer are estimated where possible from field measurement, and pumping records. The flow properties of the aquifer are estimated from field and laboratory measurements. The prediction phase of the flow is used to simulate future groundwater levels and fluxes throughout the model domain. The calibrated parameters are retained in prediction, but assumptions are made on the anticipated stresses.

4.1 Head Targets

Water levels have been measured and recorded in wells and seeps throughout the Split Rock Mill site since 1977. A total of 63 wells with 2,064 individual water table measurements were included as targets in the flow model calibration, as shown in Figure 4.1-1 and listed in Table 4.1-1. Many of these wells have long histories of water level data that provide a means to ascertain trends in water level fluctuation and gradient change.

4.2 Well Pumping and Stress Periods

Each model stress period represents a length of time in which major hydrologic stresses are considered constant. Stress periods for the calibration model were selected to accommodate the operation of pumping wells at or near the site. A review of pumping records for site wells and the two Jeffrey City supply wells (SMI, 1999; Appendix D.4.2) resulted in the designation of 58 stress periods. Because records of pumping were kept on a quarterly basis, stress period lengths are generally a multiple of 90-day intervals. A detailed breakdown of the findings and stress periods are shown in Table 4.2-1.

These listed pumping rates have been made the assigned outflows from the model aquifer, and are positioned in their representative model locations and completion intervals. All other hydrologic stresses have been assigned in the model to best approximate their estimated average values over each established stress period. The first stress period was solved as steady state in order to establish the initial potentiometric surface for the calibration run, and all other stress periods (2-58) were solved as transient.

For the predictive simulation, the only stress that is expected to change significantly in the future is the seepage from the tailings impoundment. In recognition of this, three stress periods have been designated to allow a progressive tapering of the impoundment seepage as discussed in more detail in section 4.4. The three periods run from years 2003 through 2006, 2007 through 2017, and 2017 through 3002. The only pumping represented in the predictive run was a yearly average of the Jeffrey City water supply. The initial piezometric surface for the predictive simulation is equivalent to the final surface in the calibration run.

4.3 Precipitation Recharge

To capture the variability of precipitation-derived recharge, climate data for Jeffrey City was obtained to calibrate the model recharge to actual precipitation. The National Climatic Data Center records for monthly precipitation shown in Table 4.3-1 were obtained and cover the entire calibration period. In cases where data for a particular month was absent from the record, the average for that month in all other years was substituted. When the monthly precipitation averaged over each established stress period, the result is that shown in Table 4.3-2. A recharge adjustment ratio was determined for each stress period by dividing the stress period daily average precipitation to the average daily precipitation for the entire record. These ratios were then used in the corresponding stress periods as a multiplier for previously constant model recharge rates. This assignment of recharge retains the average precipitation from previously estimates (GWPP App. E.4.4.2, 1999) yet provides the model with transient variability consistent with site conditions.

The average areal recharge rate was previously estimated to be 2 percent of precipitation (equivalent to 0.2 inches per year) has been retained in the current models. The average recharge associated with run-off from the granite outcrops, estimated to be 6.07 inches per year, was also retained. In the model, this recharge is delivered to zones of active cells that abut the inactive granite outcrops, and is scaled to account for the area of each granite sub-basin that contributes to its particular zone. Figure 4.3-1 shows the location of the zones and delineates the sub-basins.

The precipitation-derived recharge in all zones for the predictive simulations are identical to the average values discussed above.

4.4 Impoundment Recharge

An enhanced recharge zone (zone 3 in Figure 4.3-1) of constant area is used to generate the aquifer inputs in the upper valley from the Main Tailings Impoundment in the transient model. The 1977 steady state model (GWPP App. E.4.5.2.2, 1999) provided a reasonable estimate of the tailings seepage rate (608 gpm) from the Main Impoundment prior to the start of the transient simulation when the pond level is at a minimum (≈ 6365 ft.). The 1986 steady state model (GWPP App. E.4.5.2.2, 1999) provided the maximum seepage rate (1040 gpm) attained when the Main Tailings pond level was highest (≈ 6394 ft.). A linear relationship between seepage rate (y ft.³/day) and pond stage (x ft. amsl) was then established between these two endpoints:

$$y = 3434.527 \cdot x - 21762810$$

Detailed records of pond stage were then averaged over each stress period. Seepage estimates used to calculate zone 3 recharge between 1981 and 1986 are computed by evaluating this linear function for the average pond stage in each stress period.

Impoundment seepage estimates used in the transient model for stress periods after 1986 are based on the Trend Analysis of Tailings Pond Seepage Estimates previously submitted as Appendix D.f in the GWPP, which contains an expression relating seepage flow rate ($Q(t)$ in ft.³/day) to elapsed time (t in days) starting from 1986.

$$Q(t) = 698.4 + 187751 \cdot e^{-0.000506981t}$$

The impoundment seepage used to specify zone 3 model recharge for each stress period after 1986 is the value of the exponential decay expression calculated at the start of that stress period. The combined estimates are presented in Figure 4.4-1.

The exponential decay expression approaches a nearly insignificant limit of 3.6 gpm, but at the present time, and in the near future there is still appreciable seepage from the tailings impoundment. The three stress periods in the predictive simulation, as discussed in section 4.2, have been established to accommodate this diminishing seepage. The average value of the expression over each predictive stress period was used to calculate the specified model recharge in zone 3.

4.5 Specific Yield

Specific yield (S_y) is not a parameter in steady-state solutions, and thus had not been previously calibrated in the 1999 GWPP (SMI, 1999) models. In transient models, however, specific yield is used in conjunction with hydraulic conductivity to effectively determine the distance in an un-confined aquifer at which impacts from a hydraulic stress have significant effects on hydraulic head. Typically defined as the volume of water per volume of aquifer that can be drained by gravity, a higher specific yield will generally decrease the head change of a given stress at given distance. The assignment of specific yield for the calibrated flow model began with an examination of the of aquifer properties reported in Appendix C of the GWPP (SMI, 1999) to provide a representative range of S_y at the site of 0.2 to 0.35.

The steady-state model zone boundaries that had been delineated in the 1999 GWPP models in each layer for hydraulic conductivity Figures 4.5-1 through 4.5-3, have now been grouped into broader zones to represent areas of potentially distinct S_y , and are shown for layer 2 in Figure 4.5-4. Layers 1 and 3 have been configured with identical zones except where they are excluded by granite outcrop's no-flow boundaries. Specific yield and hydraulic conductivity have complimentary roles in flow model computations; thus, an initial set of conductivities was needed for estimation of specific yield. This S_y optimization was performed using the distribution of hydraulic conductivities estimated during the development of the 1999 GWPP models. The initial S_y range was used in each zone as a basis for automated parameter optimization using PEST. The resulting S_y values from this procedure minimized the discrepancy between simulated and observed heads, and were retained for the calibration of hydraulic conductivity discussed in the next section.

4.6 Calibrated Hydraulic Conductivity

Hydraulic conductivity (K_h) is the primary parameter used in mathematical models for relating the hydraulic forces applied in an aquifer to the resultant flows. This makes the accurate calibration of K_h vital to the suitability of both flow and transport models. As mentioned previously, the inverse model PEST was used in the flow calibration to assign values of K_h that produce the closest agreement between real target values and model simulation.

PEST has been used during calibration with both the zone calibration method, and the pilot-point method. Initially, an attempt was made to estimate hydraulic conductivity zones with PEST. The zone delineation was reproduced from the previous steady-state models mentioned in section 4.5 above. The only change indicated by this exercise was to increase the major hydraulic conductivity zone of the South Plain area

from 3.25 ft/day to 5.0 ft/day. This adjustment considerably improved the modeled response to pumping in the South Plain area affected by this parameter.

The PEST zone estimation method was not sufficient to adjust the hydraulic conductivity zones to obtain acceptable calibration in the Southwest Valley and the area adjacent to and outside Southwest Valley Mouth as judged by simulated vs. observed target hydrographs. This area initially contained numerous individual zones because of the high variability of the southwest valley sediments. To obtain a better calibration, these zones in layer 2 were combined into one pilot point region (Doherty, 1999 and 2000) in which PEST could vary the value of the parameter on a cell-by-cell basis, instead of having PEST estimate one value for each entire zone. Pilot points were then placed into this zone with a spacing of 1,200 ft. and PEST was allowed to estimate the hydraulic conductivity of every cell within the zone. The resulting field of conductivities for the region can be seen in Figure 4.6-1.

This final configuration provided a very good match between the historically measured heads and the transient model results. The resulting hydraulic conductivities were within the values calculated from the pumping tests and slug tests conducted in this area and reported in Appendix C of the GWPP (1999). The benefit of this approach can be seen in the fit of the calibration hydrographs shown in Figures 4.6-2 through 4.6-26. Note that the elevation scales vary among the figures to display all data with the most resolution possible.

The results of a sensitivity analysis, contained in Attachment A, indicate that the model is most sensitive to parameters that are known with a high degree of confidence, primarily hydraulic conductivities of the Southwest Valley region. Accurate matching of heads in this area is the basis for the high confidence in parameter estimates.

5.0 TRANSPORT CALIBRATION

As emphasized in the introduction of this report, the focus of the model revision was COC transport beyond the Southwest Valley Mouth. A prescribed concentration zone represents inflow of dissolved constituent to the aquifer beyond the Southwest Valley Mouth in a manner similar to the 1999 GWPP (SMI, 1999) transport models. Initial constituents down gradient of this constant concentration zone have been accounted for with a distributed field of concentrations (initial plume). Because sulfate transport is considered chemically conservative under these conditions, the aquifer system transport properties dispersivity, and porosity are optimized during sulfate transport calibration. The uranium specific transport parameter of linear distribution coefficient (K_d) is optimized during uranium transport calibration.

5.1 Transport Targets

A common collection of sulfate and uranium target wells were selected only in the areas down gradient of the prescribed source zone as listed in Table 5.1-1 and shown on Figure 5.1-1. These include older wells with good historical records of COC presence, and also more recent wells that provide higher resolution of vertical concentration gradients and current constituent migration.

5.2 Prescribed Source Zone

Constituents in the transport model are introduced to the aquifer in two ways; an initial plume representing distributed concentrations beyond the Southwest Valley mouth at the beginning of the simulation, and as a source zone from which all groundwater passing through is assigned a constant prescribed concentration of constituent. This section contains the methods used to determine how these prescribed source zones are simulated.

A cross-section was selected roughly perpendicular to each the Southwest Valley Mouth, at a location where sufficient analytical well data provided high resolution and confidence in the groundwater conditions. This basic approach was followed in previous modeling efforts (SMI, 1999; Appendix G.3.2.1). This cross-section is roughly in line with the wells WN-A, WN-B, WN-C, WELL-1, WELL-28, WELL-32A, WELL-32B, WELL-32C, SWEB-1, SWEB-2, SWEB-3, SWEB-4, and corresponds to geologic cross section J-K in Figure F-5-13 of the GWPP (SMI, 1999).

In the transport model this cross-section must be represented by a collection of model cells as shown in plan view of Figure 5.2-1. The constant concentrations are delineated into 5 separate time segments that correspond to stress periods 1-10, 11-20, 21-30, 31-40, and 41-58. The selection of time segments was chosen to best capture the changes in observed constituent concentrations at the wells within the prescribed source zone. The average (arithmetic mean) constituent concentration for each well during a given time period was used in subsequent calculations. A lateral distribution of concentration versus horizontal linear distance along the prescribed source plane was estimated for each time segment using curve-fitting software to best match the mean well concentrations. This distribution allowed the assignment of concentrations to all cells in the prescribed source zone. The base concentration assigned to each cell is generated by the curve, evaluated at the center of the cell.

Analytical data collected prior to 1996 came from samples taken from wells that were completed in multiple HSUs and, as such, did not provide sufficient information to definitively establish separate concentration estimates for the three model layers at the prescribed source zone. Reasonable evidence suggested that constituent concentrations arrive sooner in the upper HSUs and an initial vertical concentration gradient evens out as the plume matures. This is believed to be a result of the initial introduction of constituents into the upper strata of the aquifer from the impoundment area. Estimated ratios between layer concentrations are employed in the transport models to better match the arrival times of constituents in each layer. From a base concentration value determined from the concentration vs. position relationship explained above, a multiplier was used to adjust the constant source cell concentration for each layer. Starting with first time period, the layer 1 multipliers are 2.5, 2, 1.6, 1.2, and 1. Similarly for layer 2, the multipliers are 0.75, 0.8, 0.85, 0.9 and 1. These multipliers reflect the trends in concentration variation interpreted from the discrepancies of concentration between WELL-1, which is completed up to near-surface depth, and the adjacent WN-C and WN-B, which have upper completion depths that are significantly deeper. The layer-3 multiplier is 0.25 throughout, reflecting the effects from the upward nature of flow observed in this layer in the Southwest Valley Mouth that inhibits downward solute migration. Prescribed concentration zone cross sections for uranium and sulfate are depicted in Figures 5.2-2 and 5.2-3 along with their respective concentrations. For the predictive simulations, the prescribed source zone for the entire simulation was identical to the one in the fifth time segment of the calibration run.

5.3 Initial Concentrations

At the start of the calibration period there are elevated sulfate and uranium concentrations located down gradient of the modeled source. These initial concentrations are imported as a plume into the model from a Surfer® grid. Surfer is a widely used and accepted mapping and contouring software package licensed by Golden Software, Inc. The plume was created in Surfer by posting analytical sulfate data on a site map and manually contouring around the posted concentrations. The wells that supply analytical data for the 1981 initial condition are a combination of the target wells outside the Southwest Valley Mouth listed in Table 5.1-1 plus additional wells near the prescribed source zone and are listed in Table 5.3-1. Plume generation began with posted concentrations displayed on a site map. Posted concentrations for any well location, also shown in Table 5.3-1, are determined by arithmetic mean of all measured analytical data for that well over the period of 6/1/80 through 5/1/82. This time period, centered about the calibration start time of 1981, provided multiple sampling results and reduced the effect of any single concentration from biasing the resulting plumes.

The spacing of sampling wells always requires interpolation to estimate solute distribution between well locations. Contours were interpreted to honor the posted values closely, taking into account the general source location and flow direction. Well concentrations that were below the established background levels have generally been excluded from plume delineation. A lack of data directly indicating vertical constituent distribution in the early time periods required an assumed ratio of model layer 1 to layer 2 concentrations, as first discussed in section 5.2. A ratio of greater than 1 seemed warranted based on arrival timing of constituents in wells throughout the Southwest Valley mouth and plains. Several iterations of plume generation were performed in conjunction with the calibration of other transport model parameters so that the general concentration behavior of observed targets was duplicated as closely as achievable. This process is discussed in further detail for sulfate in section 5.4 and for uranium in section 5.5. The calibrated initial plumes are presented in Figures 5.3-1 through 5.3-4.

For the predictive transport simulations, new initial condition plumes for sulfate and uranium were mapped with Surfer, taking full advantage of the wealth of more recent analytical data for enhanced resolution. Concentration contours have been interpreted to accurately represent current conditions, with emphasis on representing mass in a conservative fashion in areas of conflicting or absent sample data. Figures 5.3-5 through 5.3-8 show the resulting plumes.

5.4 Effective Porosity and Dispersion

The calibration for these parameters was obtained by simulation of the sulfate transport, since sulfate is expected to behave in a chemically conservative fashion in this portion of the model. Effective porosity (n_e) is a parameter that is used in the advection-dispersion equation of transport models to calculate actual water velocity (as opposed to the Darcy or bulk velocity used in flow models). For the transport models described in this report, n_e and S_y are assumed equal. This is a common and reasonable assumption in transport modeling (McWhorter and Sunada, 1977). Zones for n_e and S_y have been set to correspond to a grouping of closely associated hydraulic conductivity zone boundaries shown in Figure 4.5-4.

Dispersion is a property associated with the non-idealities of flow in an aquifer, such as preferential flow paths, and is characterized by the parameter dispersivity (α), which has the dimension of distance (ft.). Dispersivity is typically assigned distinct longitudinal (α_L), transverse (α_T), and vertical (α_V) values relative to the direction of flow. Dispersivity was the principal transport parameter used for the calibration of the steady-state models of the 1999 GWPP, where the final estimated α_L , α_T , and α_V were 200 ft., 20 ft., and 0 ft., respectively. This result was a compromise of plume matching in the Northwest and Southwest Valleys and surroundings for both sulfate and uranium.

During the calibration of the current transport model, PEST was allowed to vary longitudinal dispersivity over the range of estimated values (20 to 800 feet) and was estimated as a single zone over the whole model domain. Only sulfate targets were used by PEST for comparison to model simulation. The α_L/α_T ratio was assumed at ten to one, as was the α_T/α_V ratio, which is a standard assumption in transport modeling (Fetter, 1999).

The results of PEST calibration indicate that α_L of 122 ft. yields the best result, while α_T and α_V have the values 12.2 ft. and 1.22 ft., respectively. This is reflected in the matching of the general trends between observed and simulated sulfate chemographs presented in Figures 5.4-1 through 5.4-16. It should be noted that where target wells are completed in multiple HSUs, simulated upper and lower layer concentrations are considered an appropriate match when they bracket the target data from above and below. This represents a non-specific well-bore dilution of water from each HSU.

5.5 Retardation of Uranium and K_d

Analytical data for sulfate and uranium concentrations at the Split Rock site demonstrate a tangible difference in transport velocities. This effect is demonstrated in the comparison of the relative concentration of uranium with that of sulfate at multiple points along the same flow path. Sulfate is regarded as a chemically conservative solute in aquifers. Uranium, conversely, often exhibits significant retardation. When sulfate and uranium concentrations are examined with respect to travel distance, there are clear patterns to suggest that the relative reductions in uranium concentration are more pronounced than relative reductions in sulfate concentrations.

From the available concentration data averaged over a period from 6/80 to 4/82 shown in Table 5.3-1, it can be seen that the sulfate concentration in WELL-3 is 81 percent of WN-C, a well up gradient and roughly along the same flow path. The same calculation for uranium yields only 58 percent. Similarly, WN-25 shows 69 percent of the sulfate concentration remaining compared to WN-B. Uranium for the same comparison of wells is at 18 percent. Further along this same flow path, WN-15 shows only 1.5 percent of the uranium concentration at WN-B, while for sulfate the percentage is 4.8 for those wells.

This trend, indicating a retarded uranium transport velocity, continues throughout the sampling history for wells outside the southwest valley mouth. Figures 5.5-1 through 5.5-7 show concentrations of sulfate and uranium on a common set of axes with uranium in concentrations of micrograms per liter and sulfate in milligrams per liter. When viewed individually, the coincidence arrival times of peaks suggest that there is little difference in travel velocities of the two constituents. This can be attributed to the temporally varying hydraulic gradients that resulted from the dissipation of the water table mound in the impoundment area, the various pumping regimes and the geometry and geology of the aquifer. The key to understanding the retardation comes from a comparison of trends at the valley mouth wells, WN-B, WN-C, to the those of wells located farther from the valley mouth, such as WELL-3, WN-24, WN-21, WN-25 and WN-15. In the former, uranium concentrations appear in the graphs as roughly twice as high as sulfate, while in the latter, sulfate is approximately equal to or less than uranium (keeping in mind these are relative and not absolute magnitudes due to the unit scales).

In MT3DMS, retardation (R) is principally controlled by assignment of the linear distribution coefficient (K_d). K_d is a parameter commonly used to characterize the equilibrium distribution of constituents between coexisting solid and aqueous phases. It is a useful parameter for characterizing the mobility of a constituent and is most often used to calculate the retardation factor. A detailed discussion of distribution

coefficient testing is presented in Appendix F.6.3 of the GWPP (SMI, 1999). The relationship between the two is:

$$R = 1 + \frac{\rho_b \cdot K_d}{n_e}$$

Where ρ_b is bulk density and n_e is porosity. Bulk density was estimated to be 1.9 g/cm³ from analysis presented in Appendix C of the GWPP (SMI, 1999). The transport parameters of porosity and dispersion have been estimated during the sulfate calibration, leaving K_d as the sole remaining parameter requiring calibration during the uranium transport simulation. It should be noted that the calibrated K_d value used in the model actually represents a lumped parameter used as an effective K_d value that incorporates numerous factors affecting the transport of each constituent. Among these factors are pH, ionic strength of the solute, number of competing cations, and permeation of the ion exchange sites of the aquifer material.

K_d was calibrated for uranium transport through a stepwise, iterative process. An initial uranium concentration plume was imported into the model. An initial estimate for K_d was specified and the model was run. Chemographs of target and simulated concentrations were scrutinized for conformity. Adjustments to the initial plume were made primarily to produce improved agreement in the early stress periods, representing a good initial condition. Specified K_d was adjusted to match the arrival and strength of concentrations in the middle and late stress periods, representing accurate transport properties. The resulting calibrated parameter lies at the lowest extreme of the laboratory estimated values and are therefore considered a conservative estimate.

The final initial plume for the calibration run is shown in Figures 5.3-3 and 5.3-4. The chemographs for uranium from the calibration phase are shown in Figures 5.5-8 through 5.5-22. The majority of concentration targets come from wells that are completed in multiple HSUs and are correspondingly assigned to multiple model layers. As discussed in section 5.4, these targets cannot provide information on vertical concentration distribution. Agreement between simulated and observed concentrations was deemed appropriate when the observed data was bracketed closely above and below by the model generated data.

6.0 PREDICTIVE TRANSPORT MODEL RESULTS

Using the calibrated parameters for transport, the initial plumes (Figures 5.3-5 through 5.3-8) and the predictive flow solution, transport simulations have been run to represent 1000 years of COC migration. The resulting distributions at 200, 500 and 1000 years are shown for sulfate in Figures 6.0-1 through 6.0-3 and for uranium in Figures 6.0-4 through 6.0-6. It should be noted that the minimum concentration shown for sulfate is 250 mg/L while that shown for uranium is 0.1 mg/L. There is a high degree of confidence in these predictions as a result of the accurate model calibration indicated by a sensitivity analysis included as Attachment A.

Based on the model predictions, a new long-term care boundary is proposed as shown in Figure 6.0-7. This boundary includes all areas that could have uranium concentrations exceeding 0.1 mg/L. The boundary limits have been selected to include only the area necessary for protection of the health and safety of the public and the environment, while maintaining a shape that is can be easily defined and monitored.

A computer compact disc is enclosed that contains a complete set of files for the revised model and the model output for the predictions.

7.0 REFERENCES

- Doherty, J. 2000. "PEST-ASP Upgrade Notes" developed by Watermark Numerical Computing, Brisbane, Australia
- Doherty, J. 1999. "PEST Model-Independent Parameter Estimation" developed by Watermark Numerical Computing, Brisbane, Australia
- Fetter, C.W., 1999. "Contaminant Hydrology." 2nd Ed., Upper Saddle River, New Jersey: Prentice Hall, Inc.
- Harbaugh, A., E. Banta, M. Hill, and M. McDonald. 2000. "MODFLOW-2000, The U.S. Geological Survey Modular Ground-Water Model – User Guide to Modularization Concepts and the Ground-Water Flow Process." U.S. Geological Survey Open File Report 00-92. Reston, Virginia.
- McWhorter, D. B., and D. Sunada, 1977. "Ground-Water Hydrology and Hydraulics." Water Resources Publications, LLC.
- Rumbaugh, J., and D. Rumbaugh, 2001. Groundwater Vistas, Version 3.09, developed by Environmental Simulations, Inc. Herndon, Virginia.
- Shepherd Miller, Inc. (SMI), 1999. "Site Closure Plan." Consultant's Report. October.
- Zheng, C., and P. Wang, 1999. *MT3DMS: A Modular Three-Dimensional Multispecies Transport Model for Simulation of Advection Dispersion and Chemical Reactions of Contaminants in Groundwater Systems; Documentation and User's Guide*. Washington D.C.

ATTACHMENT A

SENSITIVITY ANALYSIS

A sensitivity analysis was conducted on the calibrated uranium transport model. The term “sensitivity analysis” is often used to describe the technique whereby parameter values are individually varied slightly from calibration values in order to determine the effects of these changes on model predictive results. This is an unacceptable method of predictive analysis in most instances; unless parameters are varied in certain discrete ratios, the model becomes un-calibrated as soon as any parameter value is varied from its calibration value. Parameters must be varied in such a way that the objective function hardly changes. If parameters are simply incremented and/or decremented one by one, and the effect of this variation tested on both model predictions and on the objective function calculated under calibration conditions, it is likely that the latter will rise very quickly, giving the modeler the false impression that parameter values are estimated with a high degree of precision by the calibration process, and that predictive errors resulting from parameter estimate errors will be slight.

To avoid these pitfalls, a multivariate sensitivity analysis was conducted by using features of the parameter estimation package PEST. As part of parameter estimation, PEST records the overall sensitivity of each parameter, this being defined as the magnitude of the vector comprising the column of the Jacobian matrix pertaining to that parameter divided by the number of observations. Relative sensitivity is determined by multiplying the calibrated parameter's value by its overall calculated sensitivity. Relative sensitivities are provided for the calibrated flow model, the calibrated uranium transport model and a combined sensitivity for both the flow and transport model (Figures A-1, A-2, and A-3, respectively). Pilot point sensitivities (k_{ppp}) were calculated during calibration as part of the PEST estimation procedure. Estimated conductivities in model cells between these pilot points are interpolated using a kriging algorithm in the PEST program, and as such, these values could not be independently varied in the transport analysis. Values of the hydraulic conductivity zones (k_x) were varied in both the flow and transport analysis. The relative sensitivity of all parameters are included in Figure A-3, and illustrate the relative sensitivity to these parameters with respect to the uranium transport model with the exception of the afore mentioned pilot point sensitivities.

Flow Model Sensitivity

The flow model analysis indicates the model is very sensitive to conductivity estimates for seven of the twenty-four pilot points. The points are best viewed by opening the Groundwater Vistas file Calibrated Flow.gvw contained on the attached CD. Sensitivity analysis results are summarized in table A-1 and

portrayed graphically in Figure A-1. Pilot points *ppp1* and *ppp2* are located on the north side of the southwest valley. Well 3 and WN-24 are the two wells located nearest these points and the agreement of the measured head with modeled head is very good. Conductivity at this location was increased from 17 ft./day to 36.8 ft./day at *ppp1* and 95 ft./day at *ppp2*, still well within the range of conductivity measured at the facility. This agrees with the conceptual model of coarse-grained deposits in, and at the mouth of, the valleys.

Pilot point *ppp10* also shows a high degree of sensitivity. This point is situated very near WELL-1 and WELL-28, in the center of the southwest valley. These wells also display a high degree of correlation between measured and modeled heads. The degree of hydraulic conductivity variability within the southwest valley is high in both the calibrated flow model as presented in the GWPP (SMI, 1999), and the current revision.

The calculated sensitivity for pilot point 18 is high. The results for this point are enigmatic because: 1) the value is relatively unchanged from the previous version of the model and 2) the conductivity of 7.5 ft./day is similar to the pilot point estimates surrounding it. These surrounding points have a significantly lower calculated sensitivity. Nevertheless, the closest well, WN-15, shows a high degree of correlation between the measured and modeled heads, and the conductivity values are within the range measured during the field investigation.

The model is very well calibrated with respect to the transient head calibration targets. The sensitivity analysis indicates that, where calibration parameters are sensitive, transient calibration has been achieved to a high degree. Furthermore, the sensitive parameters are located in key positions of the model that either supply water to or control flow from the southwest valley. The parameter values are very similar to the values determined during the calibration of the original 1999 GWPP (SMI, 1999) steady state models. This combination of factors gives the sense of a well-calibrated flow model.

Transport Model Sensitivity

The sensitivity analysis conducted on the transport model included those parameters used in the flow model with the exception of the hydraulic conductivities determined by the pilot point PEST analysis, and the additional transport parameters of porosity (*po*), dispersivity (*al*, *at*, and *az*), and linear distribution coefficient (*kd*). The analysis is summarized in Table A-2 and illustrated in Figure A-2. Determination of the individual cell transport sensitivities for the hydraulic conductivity field generated by the pilot point

PEST optimization was not included because of the infeasible number of simulation runs required. This is not regarded, however, as jeopardizing to the analysis.

Only two parameters display significant sensitivity in the transport analysis. Hydraulic conductivity zone *Kx6517* is located at the head of the northwest valley. This zone acts to control the flux down the southwest valley. The sensitivity of this parameter in the transport model is puzzling as no contaminant is present in the northwest valley in this simulation. Presumably, this transport sensitivity is related to the flux term from the tailing pond area. If the flux were too small, modeled results would be delayed in time, as compared to measured analytical data. Conversely, too much flux down the southwest valley, and the gradient increase would cause modeled concentrations to arrive early.

The second parameter to exhibit significant sensitivity is longitudinal dispersion. It is not surprising that the transport model is sensitive to this parameter. Longitudinal dispersion directly affects the uranium transport velocity.

Kx9162 is somewhat less sensitive than the previously mentioned parameters, but worthy of mention. This parameter represents the hydraulic conductivity of the flood plain alluvium and controls the flux leaving the model to the river cells. The high relative sensitivity is due to the high parameter value of 350 ft./day. As discussed previously in this attachment, relative sensitivity is the product of the overall sensitivity multiplied by the calibrated parameter value. The fact that this calibrated parameter value is nearly an order of magnitude higher than most other conductivity zones accounts for the high relative sensitivity.

Initially, the lack of sensitivity to all *K_d* zones was perplexing. *K_d* should have nearly the same or greater sensitivity as the longitudinal dispersion parameter. Such a low sensitivity would indicate that large changes in the *K_d* parameter would not influence the results of the transport model. The relative sensitivity, as calculated by PEST, equals the calculated sensitivity multiplied by the parameter value. A careful look at the output file revealed that the calculated overall sensitivity of *K_{d10}*, the distribution coefficient in layer 2 on the south side of the southwest valley, is the third highest in the analysis. The low parameter value of 0.2 reduced the magnitude of the relative sensitivity. Since this location is where most transport occurs in the calibration simulation, the high sensitivity is expected and indicates that small variations in this parameter will cause the model to become un-calibrated.

During this analysis, it was also noticed that the parameter *Kx952*, representing a hydraulic conductivity zone in the southwest valley, also had a high calculated sensitivity and a low relative sensitivity for the same reason

Combined model sensitivity

Sensitivity calculations were also derived for the combined flow and transport calibration models. The analysis is summarized in Table A-3 and represented in Figure A-3. Only two parameters display high relative sensitivity: *Kx6517* and *Kx9162*. These parameters were the same ones that displayed high sensitivities to the transport sensitivity analysis. The high sensitivity of these values is probably related to similar causes.

Summary

The sensitivity analysis indicated that the model is well calibrated. High sensitivities exist where model results are most dependent on the value selected. Most of the sensitive parameters are situated in locations where transient calibration targets are well matched. This indicates that the values of these parameters cannot be varied greatly. Many of the parameters were determined to be relatively insensitive. This indicates that, although the values may not be as closely determined, variations in the parameters do not affect the model calibration in a significant way.

Table A-1 Flow Model Pilot Point Sensitivities

Parameter Name	Group	Current value	Sensitivity	Rel. Sensitivity
kppp1	kp	35.4989	6706.41	10396.4
kppp2	kp	100	6685.78	13371.6
kppp3	kp	92.6552	4.46E-03	8.77E-03
kppp4	kp	100	1.62E-02	3.23E-02
kppp5	kp	94.6786	7.69E-03	1.52E-02
kppp6	kp	54.5112	8.49E-03	1.47E-02
kppp7	kp	5.29767	2.11E-02	1.53E-02
kppp8	kp	100	1.69E-02	3.39E-02
kppp9	kp	39.1757	1.33E-02	2.12E-02
kppp10	kp	13.5044	6.71E+03	7.58E+03
kppp11	kp	100	1.28E-02	2.55E-02
kppp12	kp	100	1.43E-02	2.85E-02
kppp13	kp	100	1.35E-02	2.71E-02
kppp14	kp	100	1.10E-02	2.20E-02
kppp15	kp	3.7937	2.41E-02	1.39E-02
kppp16	kp	10.3668	3.31E-02	3.36E-02
kppp17	kp	100	2.84E-02	5.68E-02
kppp18	kp	7.11338	6.71E+03	5.71E+03
kppp19	kp	24.8753	6.25E-03	8.72E-03
kppp20	kp	100	6.71E+03	1.34E+04
kppp21	kp	54.6166	7.66E-03	1.33E-02
kppp22	kp	3.2372	6.69E+03	3.41E+03
kppp23	kp	1.97928	1.16E-02	3.45E-03
kppp24	kp	24.7291	6.71E+03	9.34E+03
kx5366	kx	20	2.54E-03	4.93E-02
kx3092	kx	11	1.45E-03	1.78E-02
kx276	kx	2.5	2.78E-02	8.76E-03
kx6517	kx	30	6.68E-02	0.121767
kx2407	kx	10	3.16E-02	3.27E-02
kx1447	kx	7.5	1.89E-02	3.12E-02
kx9162	kx	350	2.76E-02	8.29E-02
kx952	kx	5	0.1242	6.09E-02
kx4974	kx	17.5	2.05E-02	2.10E-02

Number of observations with non-zero weight =2918

Table A-2 Composite Transport Model Parameter Sensitivities

Parameter Name	Group	Current value	Sensitivity	Rel. Sensitivity
kx5366	kx	20	9.07E-05	1.81E-03
kx3092	kx	11	1.48E-06	1.63E-05
kx276	kx	2.5	9.46E-05	2.36E-04
kx6517	kx	30	2.61E-03	7.83E-02
kx2407	kx	10	4.47E-05	4.47E-04
kx1447	kx	7.5	3.43E-04	2.57E-03
kx9162	kx	350	8.79E-05	3.08E-02
kx952	kx	5	2.69E-03	1.35E-02
kx4974	kx	17.5	1.52E-04	2.66E-03
po2	poro	0.35	2.84E-08	9.95E-09
po3	poro	0.35	1.52E-04	5.31E-05
po4	poro	0.35	8.08E-05	2.83E-05
po5	poro	0.35	5.01E-08	1.75E-08
po6	poro	0.35	0	0
po8	poro	0.35	1.98E-04	6.92E-05
po9	poro	0.35	0	0
po10	poro	0.2	3.20E-06	6.39E-07
po12	poro	0.35	6.69E-05	2.34E-05
al1	disp	122	6.95E-04	8.48E-02
at1	disp	12.2	2.87E-05	3.50E-04
az1	disp	1.22	2.60E-05	3.17E-05
kd2	reac	0.20	4.05E-08	8.09E-09
kd3	reac	0.20	5.75E-07	1.14972E-07
kd4	reac	0.20	1.69E-04	3.38E-05
kd7	reac	0.20	0	0
kd8	reac	0.20	1.74E-04	3.49E-05
kd9	reac	0.20	2.61E-06	5.22E-07
kd10	reac	0.20	8.20E-04	1.64E-04

Number of observations with non-zero weight = 757

Table A-3 Combined Flow and Transport Composite Parameter Sensitivities

Parameter Name	Group	Current value	Sensitivity	Rel. Sensitivity
kx5366	kx	20	2.02E-03	4.03E-02
kx3092	kx	11	1.15E-03	1.27E-02
kx276	kx	2.5	2.20E-02	5.51E-02
kx6517	kx	30	5.31E-02	1.59E+00
kx2407	kx	10	2.51E-02	2.51E-01
kx1447	kx	7.5	1.50E-02	1.12E-01
kx9162	kx	350	2.20E-02	7.68E+00
kx952	kx	5	9.86E-02	4.93E-01
kx4974	kx	17.5	1.62E-02	2.84E-01
po2	poro	0.35	5.85E-09	2.05E-09
po3	poro	0.35	3.12E-05	1.09E-05
po4	poro	0.35	1.66E-05	5.82E-06
po5	poro	0.35	1.03E-08	3.61E-09
po6	poro	0.35	0	0
po8	poro	0.35	4.07E-05	1.43E-05
po9	poro	0.35	0	0
po10	poro	0.2	6.58E-07	1.32E-07
po12	poro	0.35	1.38E-05	4.82E-06
al1	disp	122	1.43E-04	1.75E-02
at1	disp	12.2	5.91E-06	7.21E-05
az1	disp	1.22	5.35E-06	6.53E-06
kd2	reac	0.20	8.34E-09	1.67E-09
kd3	reac	0.20	1.18E-07	2.37E-08
kd4	reac	0.20	3.48E-05	6.96E-06
kd7	reac	0.20	0	0
kd8	reac	0.20	3.59E-05	7.19E-06
kd9	reac	0.20	5.38E-07	1.08E-07
kd10	reac	0.20	1.69E-04	3.38E-05

Number of observations with non-zero weight = 3675

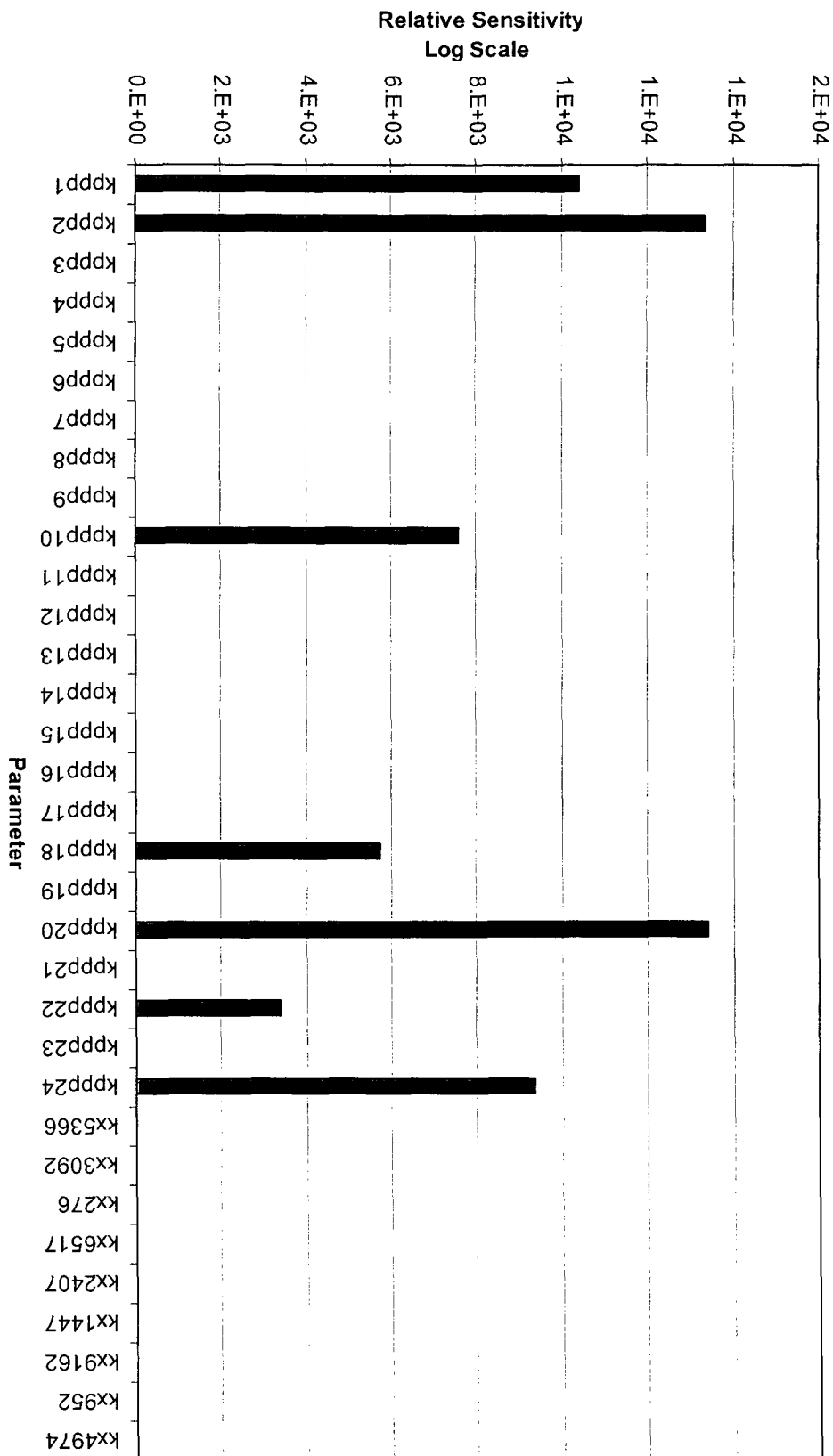


FIGURE A-1
FLOW MODEL PILOT POINT SENSITIVITIES



consulting
scientists and
engineers

Date: MARCH 2003

Project: P:\03-347\MODEL\REPORT

File: EXCEL-FIGS-A.ppt

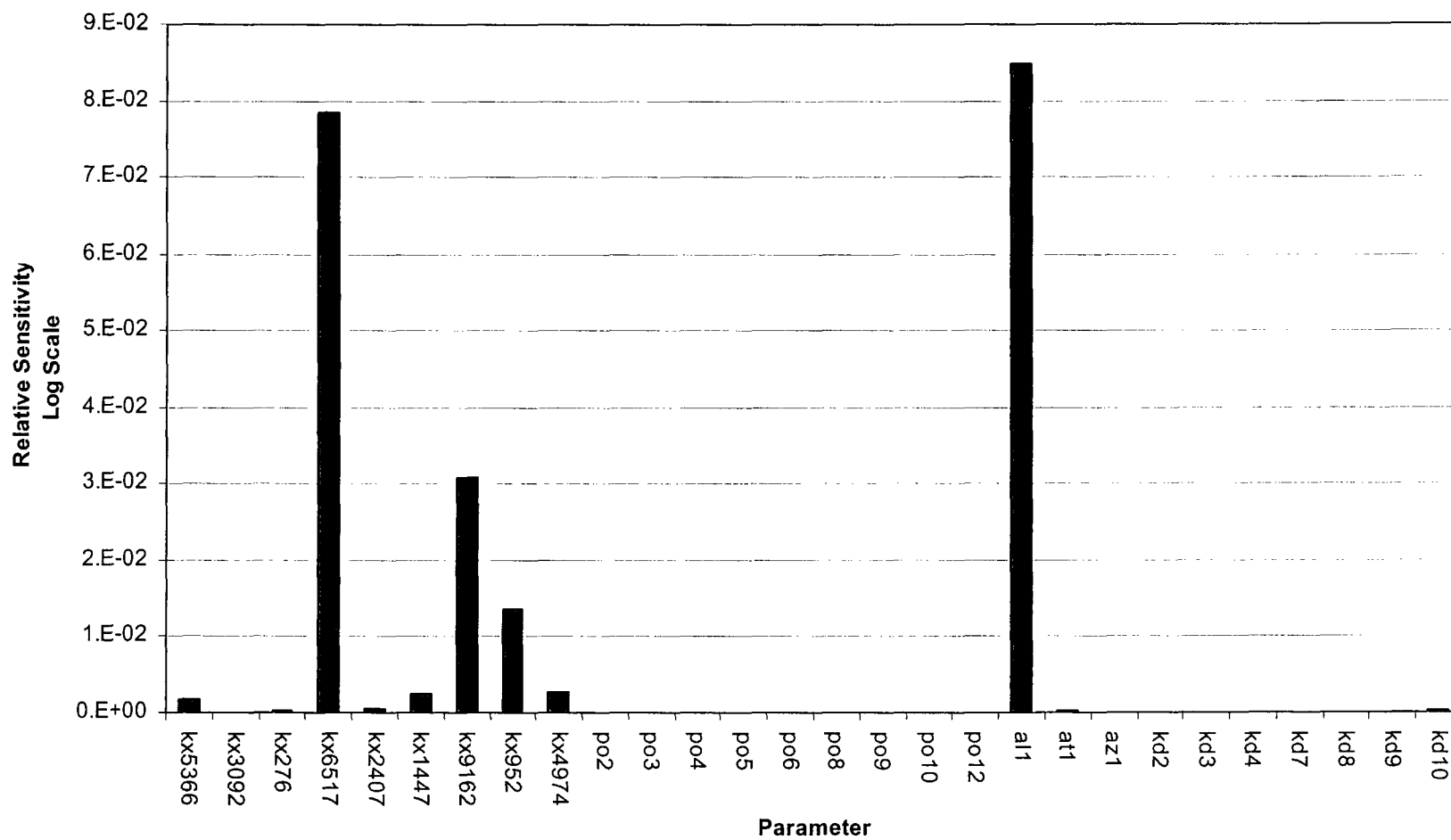


FIGURE A-2
COMPOSITE TRANSPORT MODEL PARAMETER SENSITIVITIES



consulting
scientists and
engineers

Date: MARCH 2003
Project: P:\03-347\MODEL\REPORT
File: EXCEL-FIGS-A.ppt

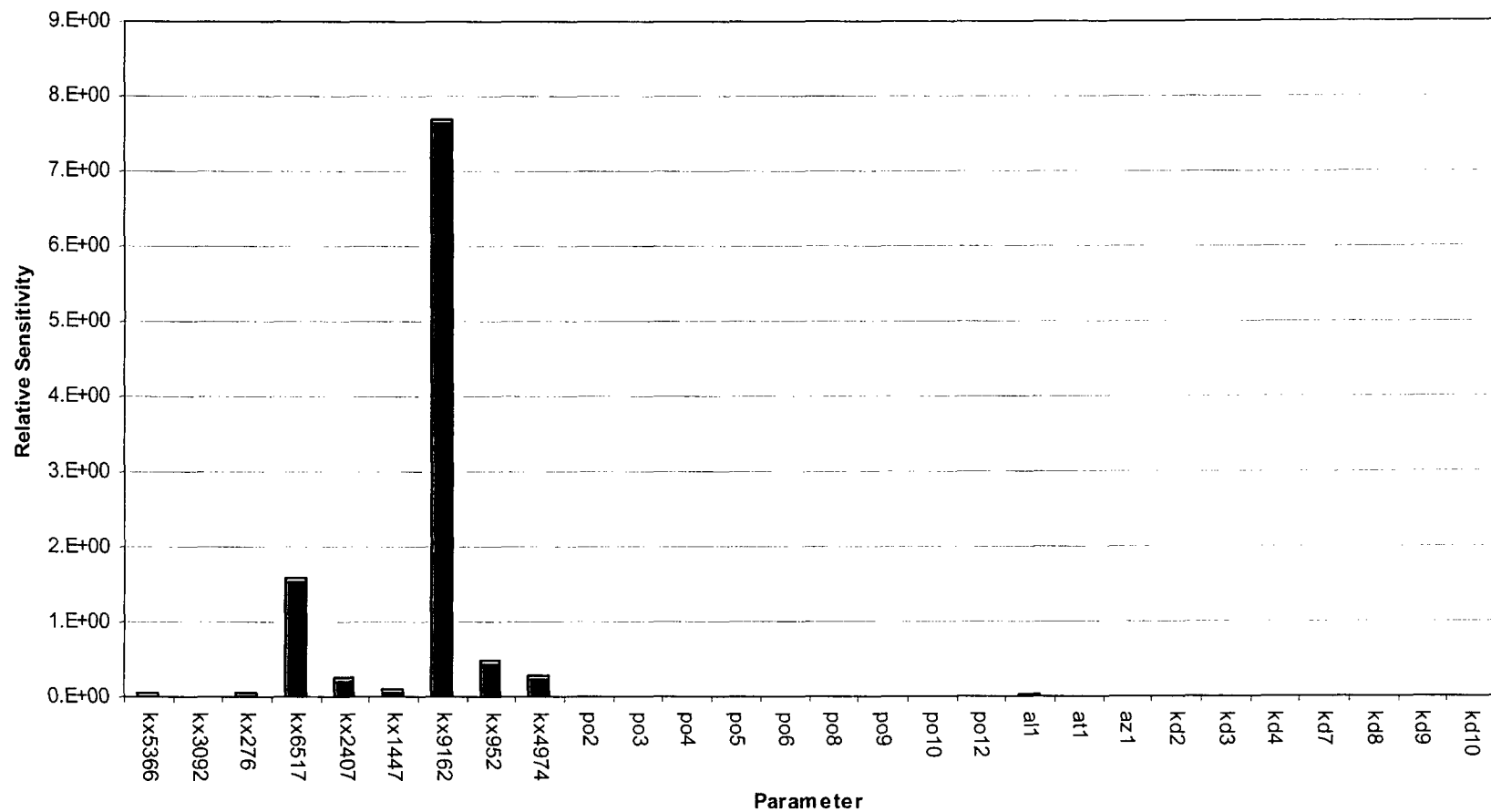


FIGURE A-3
COMBINED FLOW AND TRANSPORT
COMPOSITE PARAMETER SENSITIVITIES



consulting
scientists and
engineers

Date: MARCH 2003

Project: P:\03-347\MODEL\REPORT

File: EXCEL-FIGS-A.ppt

TABLES

Table 4.1-1 Calibration Head Targets

Name	Top of Casing Elevation	Top of Screen Depth	Bottom of Screen Depth	Model Layer	Number of Observations
ANDERSON-1	6328.42	N/A	N/A	2	3
CLAYTOR-2	6305.18	N/A	N/A	1, 2	5
CRANDELL-1	6268.12	N/A	N/A	2	3
DURBEN-1	6308.374	60	80	2	3
FOX-1	6284.66	60	80	2	2
FPEB-9	6271.94	3	293	1, 2	8
GM-2	6333.209	205	300	2	8
KNIGHT	6301.81	N/A	N/A	2	1
LP-2	6329.03	35	40	2	1
RM-1	6293.06	50	80	2	2
SAB-2	6345.72	66	86	2	8
SAB-3	6336.03	38	48	2	8
SAB-5	6349.26	33	53	2	18
SAB-8	6370.38	82.5	102.5	2	9
SWAB-14	6310.95	7.7	17.7	1, 2	19
SWAB-23	6317.92	18	28	2	12
SWAB-27	6315.72	14	24	2	10
SWAB-29	6295.03	8	18	1, 2	21
SWAB-31	6304.44	29.5	39.5	2	6
SWAB-32	6305.31	23.5	33.5	1, 2	10
SWAB-33	6287.92	18.5	28.5	2	3
SWAB-34	6293.94	22.5	32.5	2	5
SWAB-6	6316.24	12.5	22.5	1, 2	24
WELL-22	6308.74	100	260	2	11
WELL-1	6326.52	10	380	1, 2, 3	103
WELL-3	6319.72	20	140	1	99
WELL-28	6320.31	18	275	2	75
WELL-30	6305.62	15	225	2	80
WELL-4	6308.5	5	228	2	37
WELL-4E	6308.2	50	190	2	66
WELL-5	6296.02	5	230	2	97
WELL-5E	6289.4	50	230	2	79
WELL-6	6365.63	25	250	2	9
WELL-7	6343.12	5	223	2	88
WELL-9	6349.85	10	100	2	29
WELL-9E	6351	48	178	2	17

Table 4.1-1 Calibration Head Targets (Continued)

Name	Top of Casing Elevation	Top of Screen Depth	Bottom of Screen Depth	Model Layer	Number of Observations
WN-11HT	6390.53	80	153	1, 2	11
WN-13H	6353.14	5	65	1, 2	30
WN-15	6338.62	18	298	1, 2	75
WN-16	6307.19	15	315	1, 2	74
WN-17	6285.92	11	71	2	83
WN-18	6282.2	20	180	1, 2	85
WN-19	6273.9	2.5	60.8	2	65
WN-20	6399.91	71	211	1, 2	9
WN-21	6316.49	2.7	322	1, 2	99
WN-23	6280.5	10.5	70.5	1, 2	81
WN-24	6319	2.7	282	1, 2	83
WN-25	6313.62	11	191	1, 2	97
WN-26	6313.3	71.5	111.5	2	59
WN-3S	6365.31	21.4	23.4	1, 2	5
WN-38C	6271.93	12	27	1, 2	15
WN-40C	6278.94	4.5	19.5	1	20
WN-41C	6277.37	5	15	1	18
WN-43B	6287.49	33.45	53.45	2	15
WN-43C	6288	4.5	19.5	1	19
WN-4HAT	6308.4	18	20	1	14
WN-6S	6387.02	36.1	38.1	1, 2	9
Total Number of Observations					1945

Table 4.2-1 Well Pumping and Stress Period Designation

Stress Period	Period Length (days)	Elapsed time (days)	Ending Date	Action	Pumping Rate								Townsite Water Supply Wells (GPM)
					Well#2 (GPM)	WN-A (GPM)	WN-B (GPM)	WN-C (GPM)	4E (GPM)	9E (GPM)	5E (GPM)	WN-B (GPM)	
1	183	183	4/2/1981	MO	1425								152.6
2	91	274	7/2/1981	MO	1425								587.6
3	91	365	10/1/1981	ES	650								587.6
4	91	457	1/1/1982	ES	650								152.6
5	91	548	4/2/1982	ES	650								150
6	183	731	10/1/1982	ES	650								480
7	183	913	4/2/1983	ES	650								150
8	183	1096	10/2/1983	ES	650								480
9	91	1187	1/1/1984	ES	650								150
10	91	1278	4/1/1984	P	650	50	50	50					150
11	183	1461	10/1/1984	P	650	50	50	50					480
12	183	1644	4/2/1985	P	650	50	50	50					150
13	183	1826	10/1/1985	P	650	50	50	50					480
14	183	2009	4/2/1986	P	650	50	50	50					150
15	183	2192	10/1/1986	P	650	50	50	50					365
16	91	2283	1/1/1987	MTD	45								150
17	91	2374	4/2/1987										150
18	183	2557	10/2/1987										365
19	183	2739	4/1/1988										150
20	183	2922	10/1/1988										365
21	183	3105	4/2/1989										150
22	183	3287	10/1/1989										365
23	91	3379	1/1/1990										150
24	91	3470	4/2/1990	CAP					38	38			150
25	183	3653	10/1/1990	CAP					40	40	40	40	365
26	183	3835	4/2/1991	CAP					29.4	30			150
27	183	4018	10/2/1991	CAP					101	101			365

Table 4.2-1 Well Pumping and Stress Period Designation (Continued)

Stress Period	Period Length (days)	Elapsed time (days)	Ending Date	Action	Pumping Rate								Townsite Water Supply Wells (GPM)
					Well#2 (GPM)	WN-A (GPM)	WN-B (GPM)	WN-C (GPM)	4E (GPM)	9E (GPM)	5E (GPM)	WN-B (GPM)	
28	91	4109	1/1/1992	CAP					30.7	32.5			45
29	91	4200	4/1/1992	CAP									45
30	183	4383	10/1/1992	CAP					54	54	54	54	130
31	183	4566	4/2/1993	CAP									45
32	183	4748	10/1/1993	CAP					47.5	47.5	47.5	47.5	130
33	183	4931	4/2/1994	CAP									45
34	183	5114	10/1/1994	CAP					52.5	52.5	52.5	52.5	130
35	183	5296	4/2/1995	CAP									45
36	91	5387	7/2/1995	CAP					66.7	66.7	66.7	66.7	130
37	91	5479	10/2/1995	CAP									130
38	183	5661	4/1/1996	CAP									45
39	91	5753	7/2/1996	CAP									130
40	91	5844	10/1/1996	CAP					62.5		30	62.5	130
41	183	6027	4/2/1997	CAP									45
42	91	6118	7/2/1997	CAP					64.8			55.2	130
43	91	6209	10/1/1997	CAP									130
44	183	6392	4/2/1998	CAP									45
45	91	6483	7/2/1998	CAP					62			53.6	130
46	91	6575	10/1/1998	CAP									130
47	183	6757	4/2/1999	CAP									45
48	91	6848	7/2/1999	CAP					58.5			49.3	130
49	91	6940	10/2/1999	CAP									130
50	183	7122	4/1/2000	CAP									45
51	91	7214	7/2/2000	CAP					52.7			46.6	130
52	91	7305	10/1/2000	CAP									130
53	183	7488	4/2/2001	CAP									45

Table 4.2-1 Well Pumping and Stress Period Designation (Continued)

Stress Period	Period Length (days)	Elapsed time (days)	Ending Date	Action	Pumping Rate								
					Well#2 (GPM)	WN-A (GPM)	WN-B (GPM)	WN-C (GPM)	4E (GPM)	9E (GPM)	5E (GPM)	WN-B (GPM)	Townsite Water Supply Wells (GPM)
54	91	7579	7/2/2001	CAP					54			46	130
55	91	7670	10/1/2001	CAP									130
56	183	7853	4/2/2002	CAP									45
57	91	7944	7/2/2002	CAP					54			46	130
58	91	8036	10/1/2002										130

MO = Main Ops

ES = Early Standby

P = Pumpback

MTD = Main Tailing Drainage

CAP

Table 4.3-1 Jeffrey City Monthly Precipitation Record

YEAR	JAN	FEB	MAR	APR	MAY	JUN	JUL	AUG	SEP	OCT	NOV	DEC	ANNUAL TOTAL
1964	38	38	84	126	273	120	34	42	24	20	33	5	837
1965	14	27	8	103	380	138	92	47	127	17	3	85	1041
1966	38	61	62	47	62	84	120	138	82	74	69	44	881
1978	38	38	84	126	217	116	92	66	67	15	72	128	1059
1979	74	15	111	132	204	96	23	169	4	49	74	56	1007
1980	73	8	92	93	341	18	5	80	21	90	55	14	890
1981	11	48	60	106	405	0	142	54	7	48	24	27	932
1982	16	26	43	45	167	164	97	31	249	141	47	77	1103
1983	32	26	149	246	173	282	39	28	27	52	269	92	1415
1984	79	36	90	192	178	117	333	205	66	20	23	44	1383
1985	53	49	78	50	163	214	116	19	118	10	87	95	1052
1986	9	67	181	213	172	129	77	67	86	185	50	55	1291
1987	91	74	66	51	267	220	79	145	65	98	57	67	1280
1988	35	38	160	74	170	18	7	65	105	0	0	55	727
1989	0	93	15	17	212	110	103	90	213	19	0	28	900
1990	16	0	112	110	123	56	202	20	132	21	142	33	967
1991	18	32	28	108	347	154	27	15	91	122	119	6	1067
1992	35	33	106	116	360	99	199	58	24	6	78	60	1174
1993	63	33	144	144	162	237	106	32	90	156	121	35	1323
1994	51	23	70	99	22	15	62	19	14	295	126	7	803
1995	66	41	51	169	493	127	68	7	75	127	71	17	1312
1996	31	27	87	97	217	29	33	44	67	116	64	29	841
1997	43	41	28	162	218	171	128	162	131	62	17	80	1243
1998	12	30	235	144	73	301	163	46	53	184	55	7	1303
1999	47	39	11	402	263	47	8	61	91	60	11	11	1051
2000	9	25	82	96	190	63	101	54	137	7	111	15	890
2001	24	84	24	138	95	28	66	27	37	13	75	9	620
2002	21	9	84	134	137	85	49	66	82	74	69	44	854

Bold numbers are calculated values based on NCDC records, but are not supplied by NCDC. - see text for calculations

All values are 1/100 inch

Table 4.3-2 Precipitation Recharge Adjustment Ratio

Stress Period Start Date	Stress Period	Stress Period Length (day)	Total Period Precipitation (0.01 in.)	Stress Period Daily Average Precipitation (0.01 in.)	Recharge Adjustment Ratio
January 1, 1978		91	159	1.75	0.59
April 2, 1978		183	685	3.75	1.26
October 1, 1978		183	415	2.27	0.76
April 2, 1979		183	628	3.44	1.16
October 2, 1979		183	352	1.93	0.65
April 1, 1980		183	558	3.06	1.03
October 1, 1980	1	183	278	1.52	0.51
April 2, 1981	2	91	511	5.60	1.88
July 2, 1981	3	91	203	2.22	0.75
October 1, 1981	4	91	99	1.08	0.36
January 1, 1982	5	91	85	0.93	0.31
April 2, 1982	6	183	753	4.12	1.39
October 1, 1982	7	183	472	2.58	0.87
April 2, 1983	8	183	795	4.35	1.47
October 2, 1983	9	91	413	4.52	1.52
January 1, 1984	10	91	205	2.25	0.76
April 1, 1984	11	183	1091	5.97	2.01
October 1, 1984	12	183	267	1.46	0.49
April 2, 1985	13	183	680	3.72	1.25
October 1, 1985	14	183	449	2.46	0.83
April 2, 1986	15	183	744	4.07	1.37
October 1, 1986	16	91	290	3.18	1.07
January 1, 1987	17	91	231	2.53	0.85
April 2, 1987	18	183	827	4.53	1.52
October 2, 1987	19	183	455	2.49	0.84
April 1, 1988	20	183	439	2.40	0.81
October 1, 1988	21	183	163	0.89	0.30
April 2, 1989	22	183	745	4.08	1.37
October 1, 1989	23	91	47	0.51	0.17
January 1, 1990	24	91	128	1.40	0.47
April 2, 1990	25	183	643	3.52	1.18
October 1, 1990	26	183	274	1.50	0.50
April 2, 1991	27	183	742	4.06	1.37
October 2, 1991	28	91	247	2.70	0.91
January 1, 1992	29	91	174	1.91	0.64
April 1, 1992	30	183	856	4.69	1.58
October 1, 1992	31	183	384	2.10	0.71
April 2, 1993	32	183	771	4.22	1.42
October 1, 1993	33	183	456	2.50	0.84

Table 4.3-2 Precipitation Recharge Adjustment Ratio (Continued)

Stress Period Start Date	Stress Period	Stress Period Length (day)	Total Period Precipitation (0.01 in.)	Stress Period Daily Average Precipitation (0.01 in.)	Recharge Adjustment Ratio
April 2, 1994	34	183	231	1.26	0.43
October 1, 1994	35	183	586	3.21	1.08
April 2, 1995	36	91	789	8.64	2.91
July 2, 1995	37	91	150	1.64	0.55
October 2, 1995	38	183	360	1.97	0.66
April 1, 1996	39	91	343	3.76	1.26
July 2, 1996	40	91	144	1.58	0.53
October 1, 1996	41	183	321	1.76	0.59
April 2, 1997	42	91	551	6.03	2.03
July 2, 1997	43	91	421	4.61	1.55
October 1, 1997	44	183	436	2.39	0.80
April 2, 1998	45	91	518	5.67	1.91
July 2, 1998	46	91	262	2.87	0.97
October 1, 1998	47	183	343	1.88	0.63
April 2, 1999	48	91	712	7.80	2.62
July 2, 1999	49	91	160	1.75	0.59
October 2, 1999	50	183	198	1.08	0.36
April 1, 2000	51	91	349	3.82	1.29
July 2, 2000	52	91	292	3.20	1.08
October 1, 2000	53	183	265	1.45	0.49
April 2, 2001	54	91	261	2.86	0.96
July 2, 2001	55	91	130	1.42	0.48
October 1, 2001	56	183	211	1.16	0.39
April 2, 2002	57	91	356	3.90	1.31
July 2, 2002	58	91	198	2.16	0.73
Total Daily average Precipitation (0.01 in.)				2.97	

Table 5.1-1 Concentration Target Wells

Name	Top of Casing Elevation	Top of Screen Depth	Bottom of Screen Depth	Model Layer	Sulfate targets	Uranium targets
SWAB-1	6321.31	17.5	27.5	1	5	5
SWAB-10	6317.79	19.5	29.5	1	4	4
SWAB-11	6314.76	15.1	25.1	1	4	4
SWAB-15	6306.23	12.1	22.1	1	6	6
SWAB-3	6314.65	13.2	23.2	1,2	4	4
SWAB-7	6305.03	9.8	19.8	1	5	5
SWAB-8	6325.3	24.8	34.3	1,2	5	5
SWEB-11	6307.31	380	400	2	3	3
SWEB-12	6305.22	460	480	2	5	5
SWEB-6	6320.49	N/A*	N/A*	2	4	4
SWEB-8	6320.95	163.76	183.76	2	3	4
WELL-3	6319.72	20	140	1,2	95	74
WN-15	6338.62	18	298	1,2	80	58
WN-21	6316.49	2.7	322	1,2	97	76
WN-24	6319	2.7	282	1,2	96	74
WN-25	6313.62	11	191	1,2	95	74

* Casing not perforated, total depth 398

Table 5.3-1 Initial Concentration Plume Wells

Well ID	Sulfate (mg/L)	Uranium (ug/L)
WN-A	1132	827
WN-B	2116	4765
WN-C	1112	2500
WELL-1	3441	6143
WELL-10	32	8
WELL-3	905	1450
WN-13H	3918	113
WN-15	102	72
WN-1HDA	3140	1446
WN-21	81	30
WN-16	25	52
WN-22	35	72
WN-25	1457	876
WN-24	46	13

FIGURES



LEGEND

NO FLOW CELLS

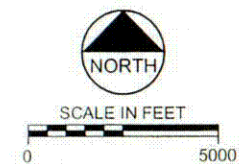
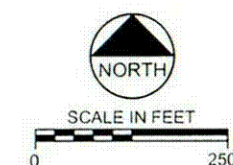
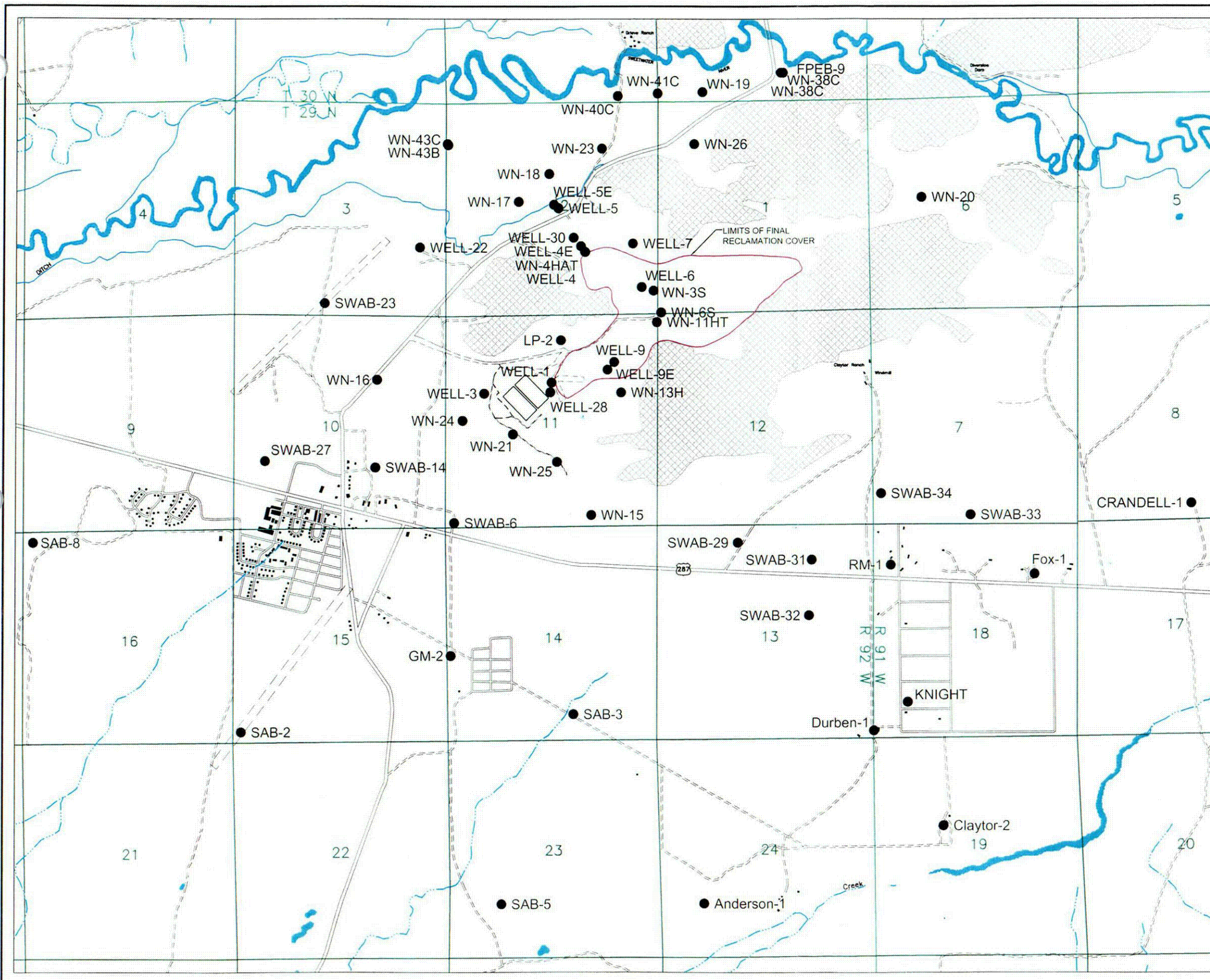


FIGURE 3.6-1
MODEL DOMAIN AND GRID



Date: MARCH 2003
Project: 003347
File: DOMAIN-01.DWG

C01



C02

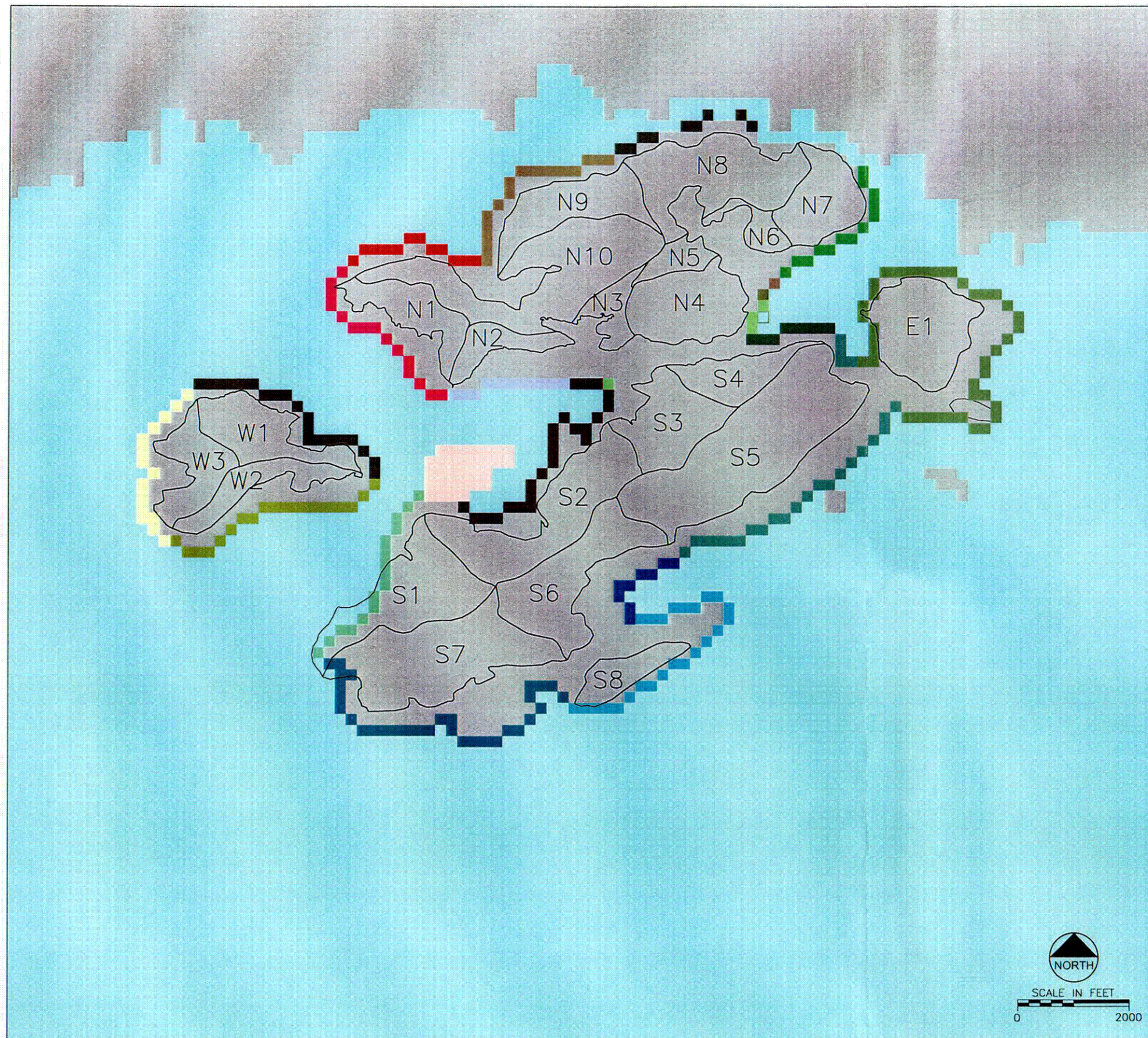
FIGURE 4.1-1
HEAD TARGET WELL LOCATIONS



Date:	MARCH 2003
Project:	003347
File:	WELLS-01.DWG

14770033 Wells-01.dwg
Date: 2003
Time: 10:57

\\nasdaq1\env\3 457\2003\03\GIS\434\0315.dwg
Date: 3/12/03
Time: 12:01



Basin	Recharge Zones	Basin Recharge (in/yr)	Basin Drainage Area (sq. ft.)	Model Recharge (ft/d)	Model Area (sq. ft.)	Model Recharge (gpm)
■ W1	5	6.07	1,955,871	3.386E-03	800,000	14.1
■ W2	6	6.07	1,269,596	2.442E-03	720,000	9.1
■ W3	7	6.07	1,533,803	3.540E-03	600,000	11.0
■ N1	8	6.07	1,556,236	3.592E-03	600,000	11.2
■ N2	9	6.07	916,129	2.884E-03	440,000	6.6
■ N3	10	6.07	757,116	8.738E-03	120,000	5.4
■ N4	11	6.07	2,467,845	2.136E-02	160,000	17.8
■ N5	12	6.07	624,053	2.161E-02	40,000	4.5
■ N6	13	6.07	574,463	1.989E-02	40,000	4.1
■ N7	14	6.07	1,832,284	4.880E-03	520,000	13.2
■ N8	15	6.07	3,361,595	1.293E-02	360,000	24.2
■ N9	16	6.07	2,107,702	4.293E-03	680,000	15.2
■ N10	17	6.07	4,666,569	1.346E-02	480,000	33.6
■ S1	18	6.07	3,239,373	6.597E-03	680,000	23.3
■ S2	19	6.07	3,607,969	7.807E-03	640,000	26.0
■ S3	20	6.07	2,197,960	3.805E-02	80,000	15.8
■ S4	21	6.07	1,337,914	5.790E-03	320,000	9.6
■ S5	22	6.07	6,133,123	8.494E-03	1,000,000	44.1
■ S6	23	6.07	3,601,215	1.559E-02	320,000	25.9
■ S7	24	6.07	4,937,225	5.342E-03	1,280,000	35.5
■ S8	26	6.07	1,005,128	1.450E-03	960,000	7.2
■ E1	25	6.07	2,812,225	2.950E-03	1,320,000	20.2
■ AREAL	2	0.17		3.880E-05	839,896,000	169.3
1996 TAILING	3				1,240,000	

FIGURE 4.3-1
MODEL RECHARGE ZONES

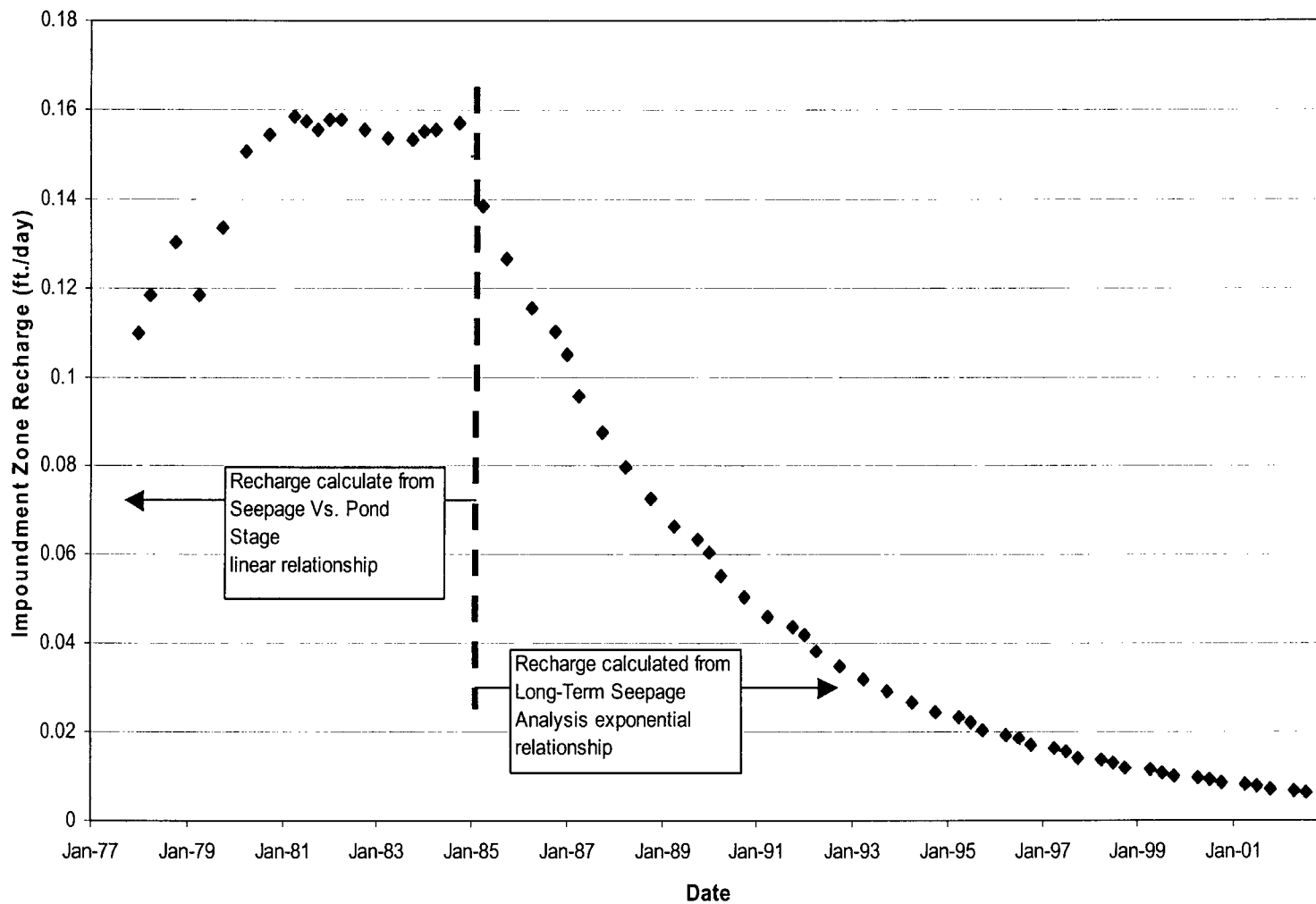


Date: MARCH 2003

Project: 003347

File: RECHAREZONES.DWG

C03



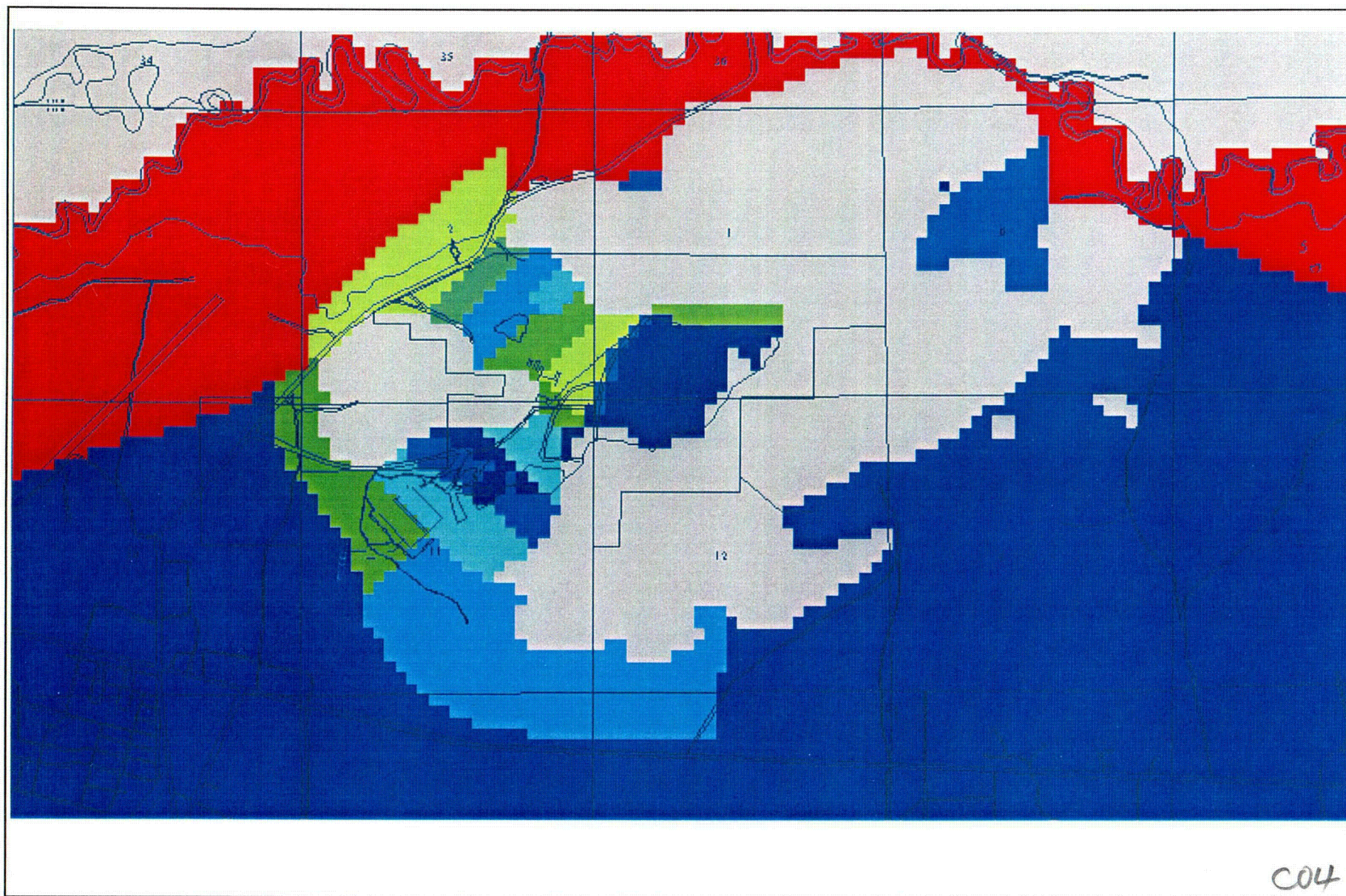
consulting
scientists and
engineers

FIGURE 4.4-1
IMPOUNDMENT SEEPAGE RECHARGE ESTIMATE

Date: MARCH 2003

Project: P:\03-347\MODEL\REPORT

File: EXCEL-FIGS-4.ppt



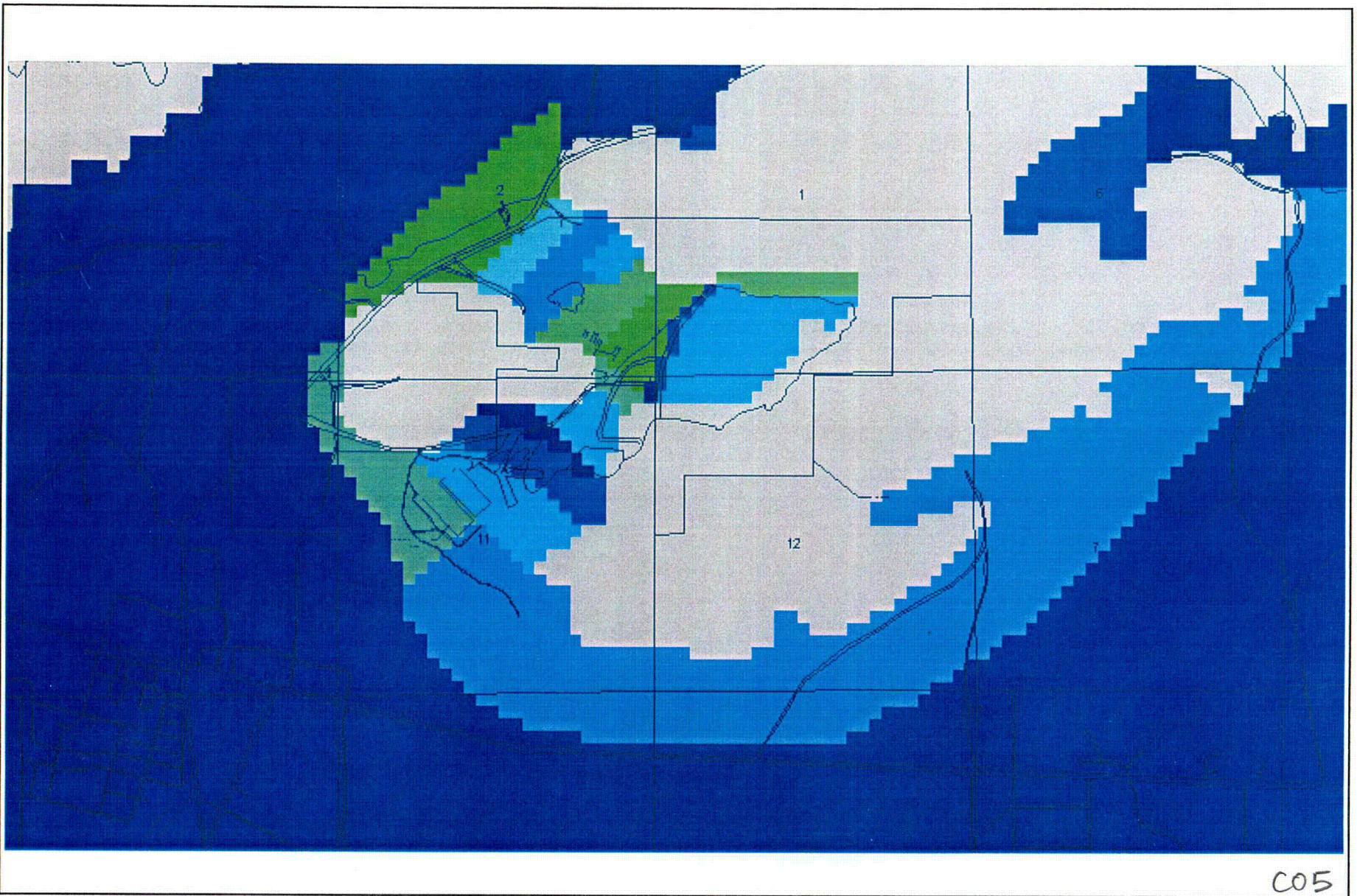
consulting
scientists and
engineers

Figure 4.5-1
Hydraulic Conductivity Zone Boundaries, Layer 1

Date: MARCH 2003

Project: 003347\2003

File: SWV HYD.....PPT



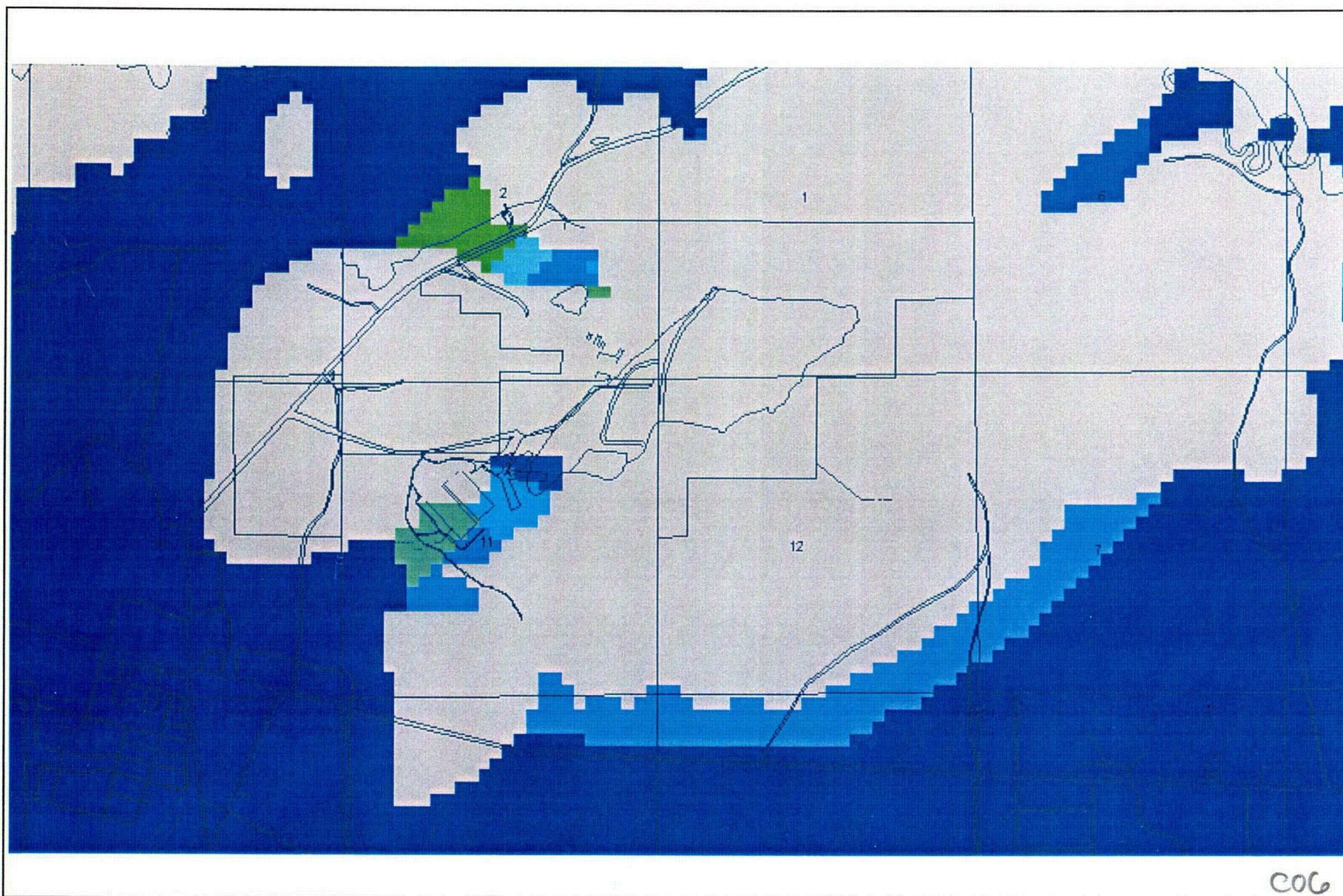
consulting
scientists and
engineers

Figure 4.5-2
Hydraulic Conductivity Zone Boundaries, Layer 2

Date: MARCH 2003

Project: 003347\2003

File: SWV HYD.....PPT



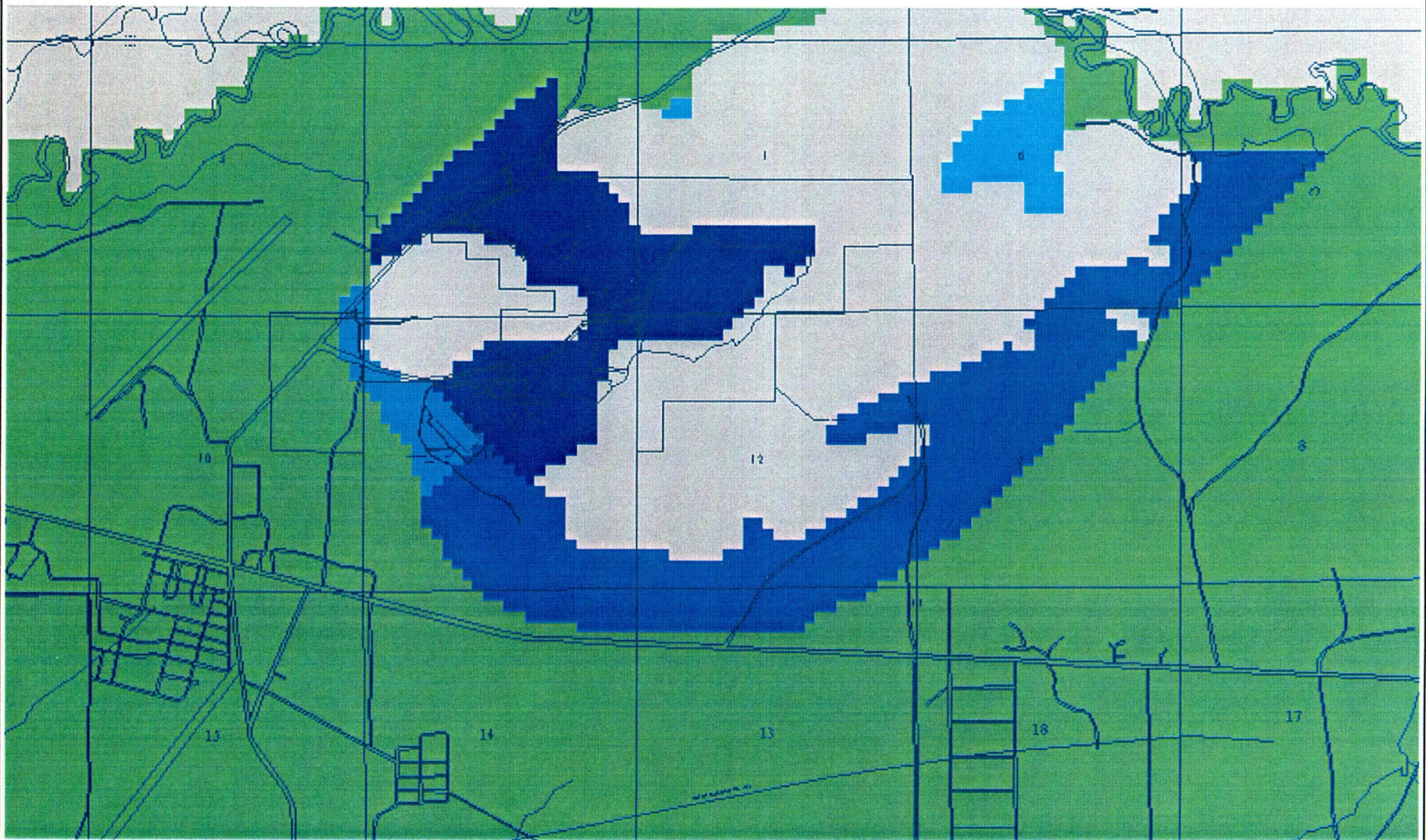
consulting
scientists and
engineers

Figure 4.5-3
Hydraulic Conductivity Zone Boundaries, Layer 3

Date: MARCH 2003

Project: 003347\2003

File: SWV HYD.....PPT



C07



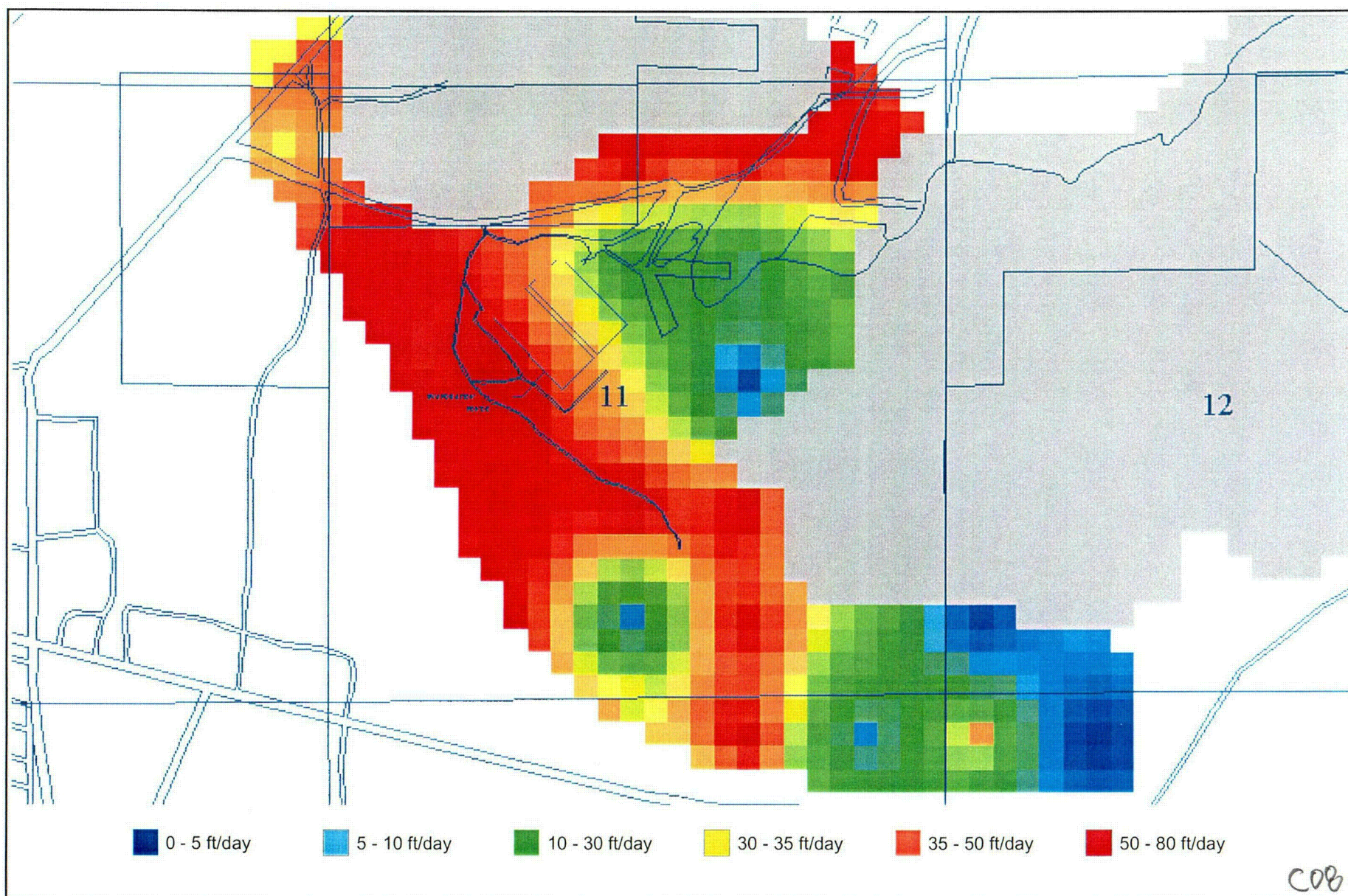
consulting
scientists and
engineers

Figure 4.5-4
Specific Yield/Porosity Zone Boundaries

Date: MARCH 2003

Project: 003347/2003

File: SWV HYD.....PPT



consulting
scientists and
engineers

Figure 4.6-1
Calibrated Hydraulic Conductivity, Southwest Valley Region

Date: MARCH 2003

Project: 003347\2003

File: SWV HYD.....PPT

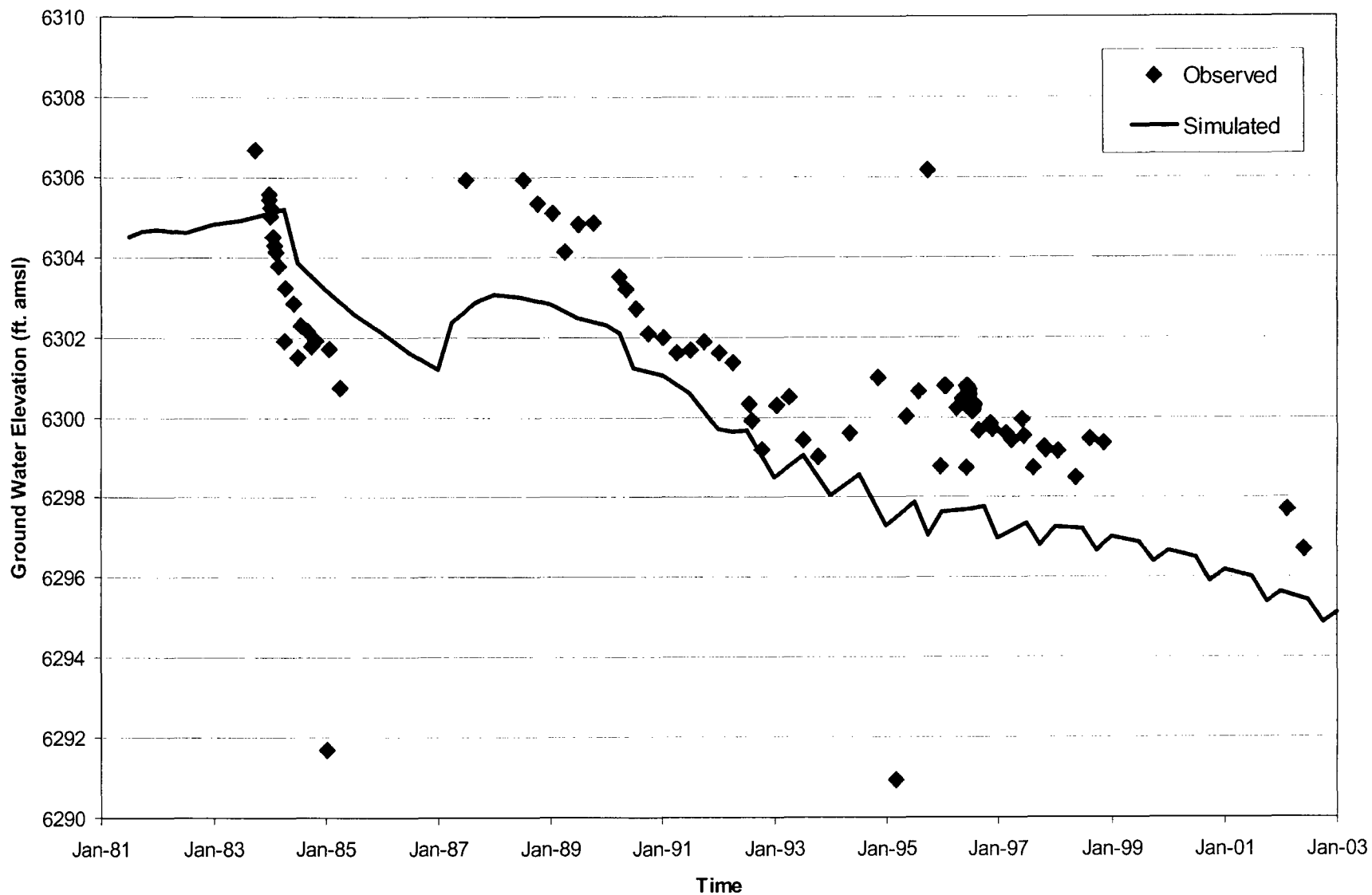


FIGURE 4.6-2
WELL-1 OBSERVED vs. SIMULATED
GROUND WATER HYDROGRAPH



consulting
scientists and
engineers

Date: MARCH 2003

Project: P:\03-347\MODEL\REPORT

File: EXCEL-FIGS-4.ppt

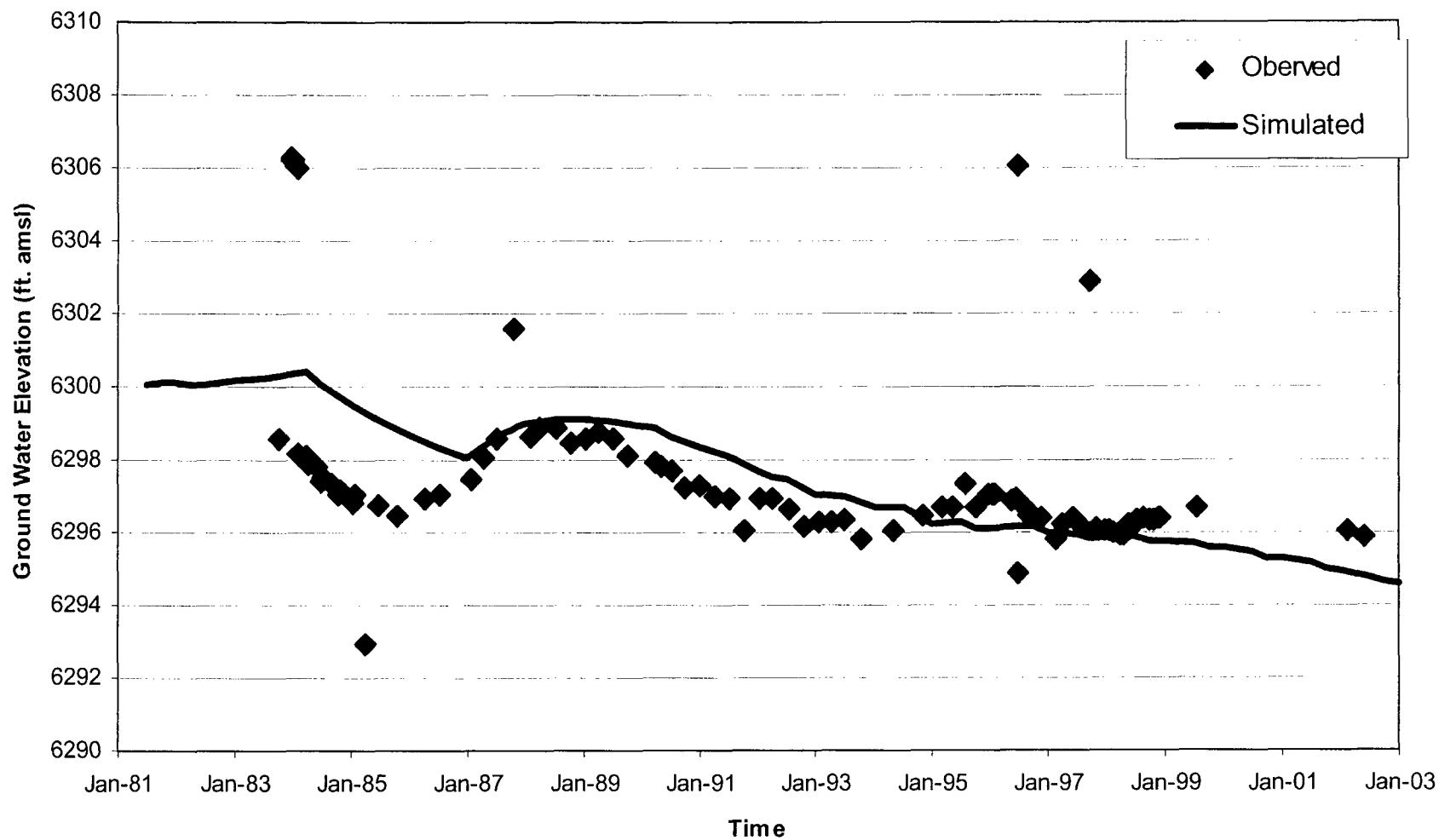


FIGURE 4.6-3
WELL-3 OBSERVED vs. SIMULATED
GROUND WATER HYDROGRAPH



consulting
scientists and
engineers

Date: MARCH 2003

Project: P:\03-347\MODEL\REPORT

File: EXCEL-FIGS-4.ppt

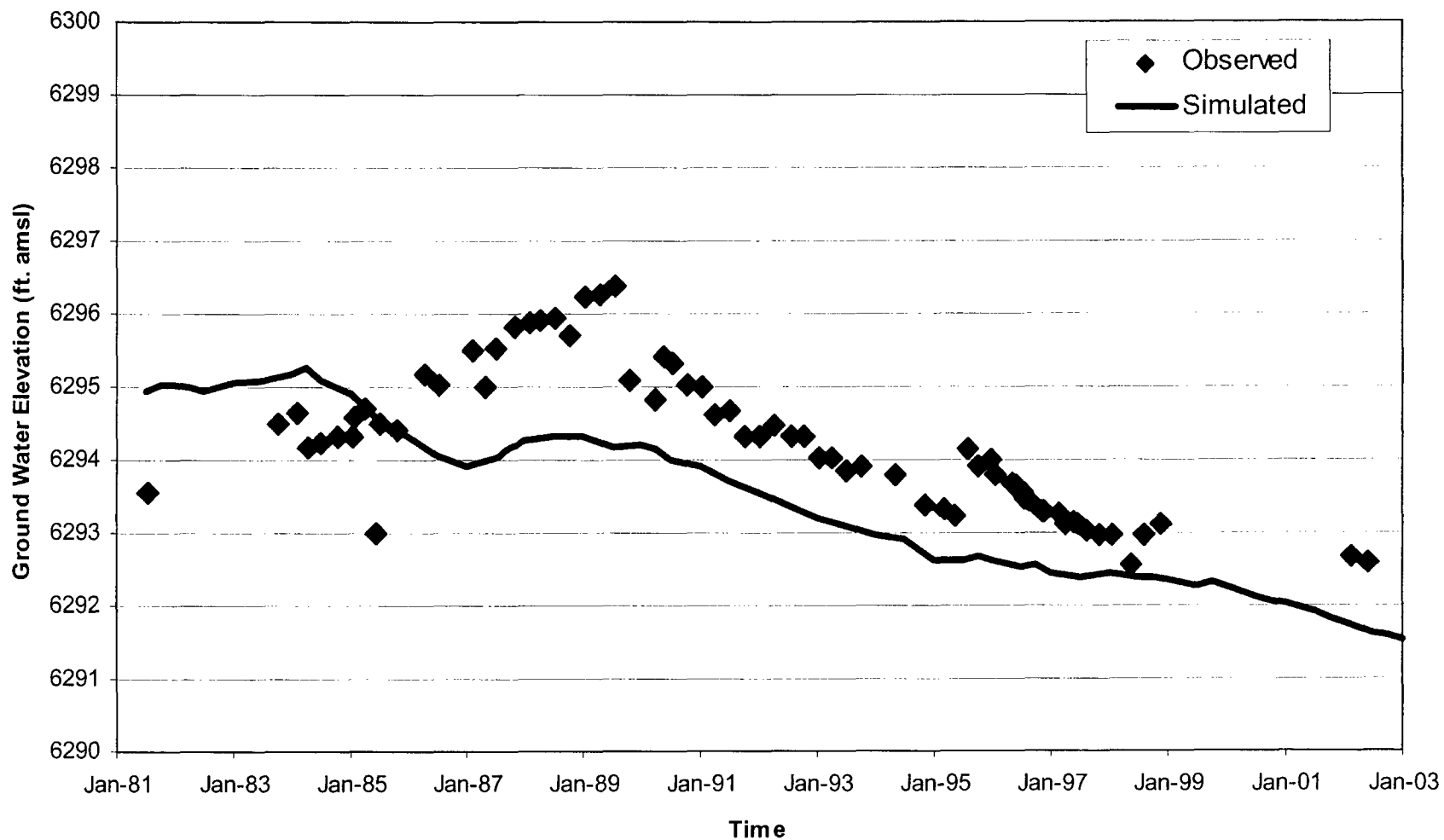


FIGURE 4.6-4
WN-15 OBSERVED vs. SIMULATED
GROUND WATER HYDROGRAPH



consulting
scientists and
engineers

Date: MARCH 2003

Project: P:\03-347\MODEL\REPORT

File: EXCEL-FIGS-4.ppt

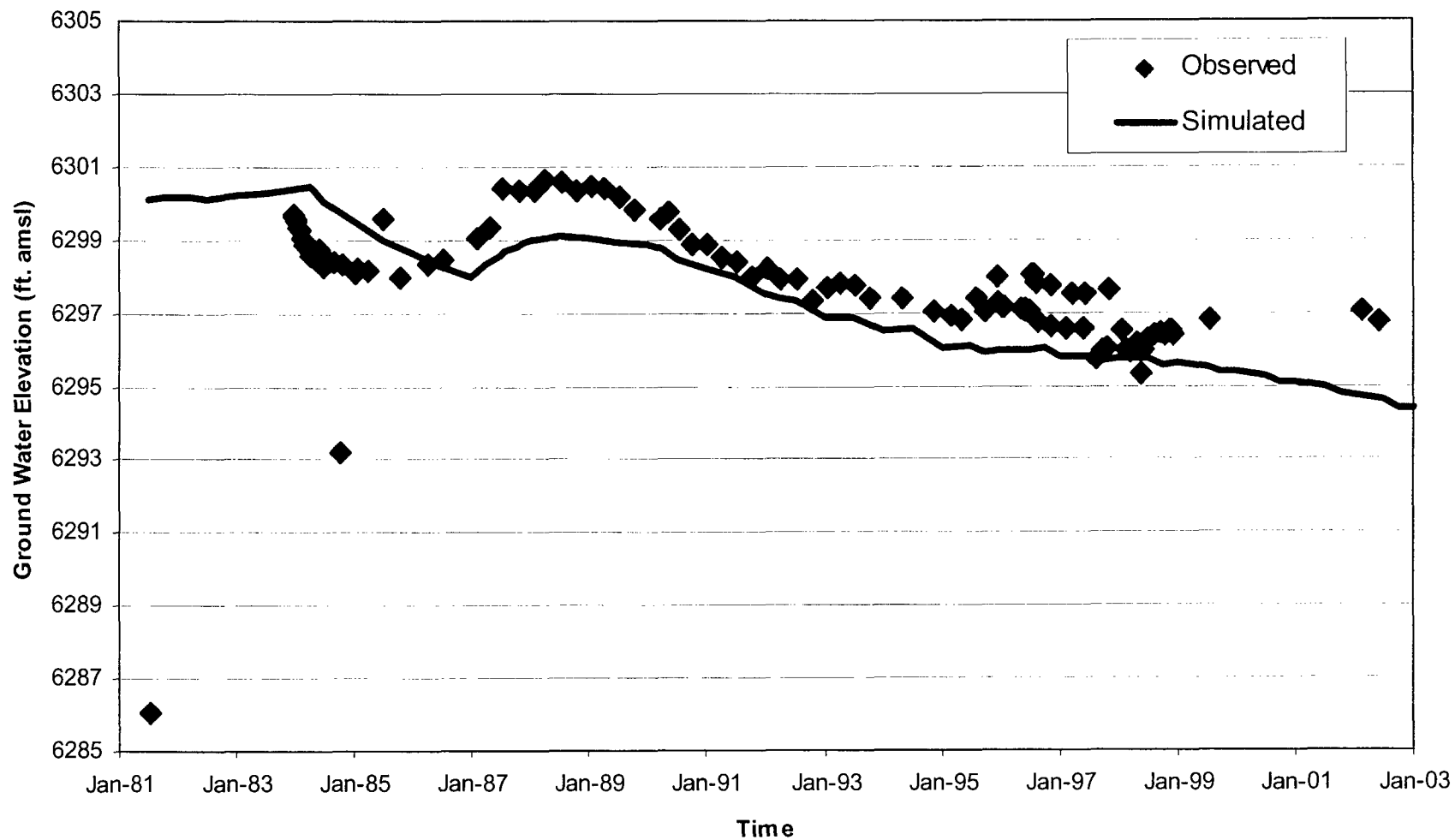


FIGURE 4.6-5
WN-21 OBSERVED vs. SIMULATED
GROUND WATER HYDROGRAPH



consulting
scientists and
engineers

Date: MARCH 2003

Project: P:\03-347\MODEL\REPORT

File: EXCEL-FIGS-4.ppt

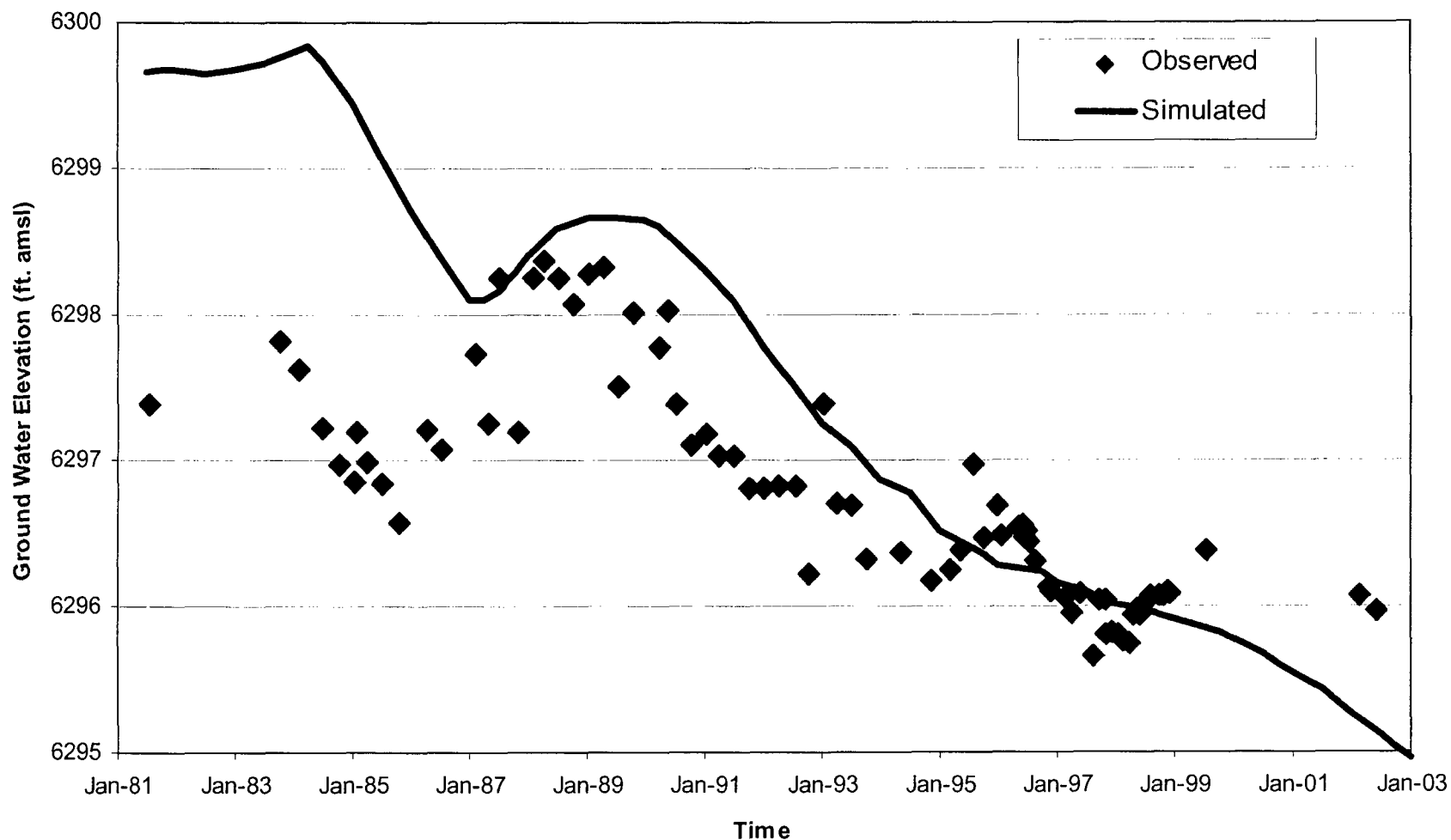


FIGURE 4.6-6
WN-24 OBSERVED vs. SIMULATED
GROUND WATER HYDROGRAPH



consulting
scientists and
engineers

Date: MARCH 2003

Project: P:\03-347\MODEL\REPORT

File: EXCEL-FIGS-4.ppt

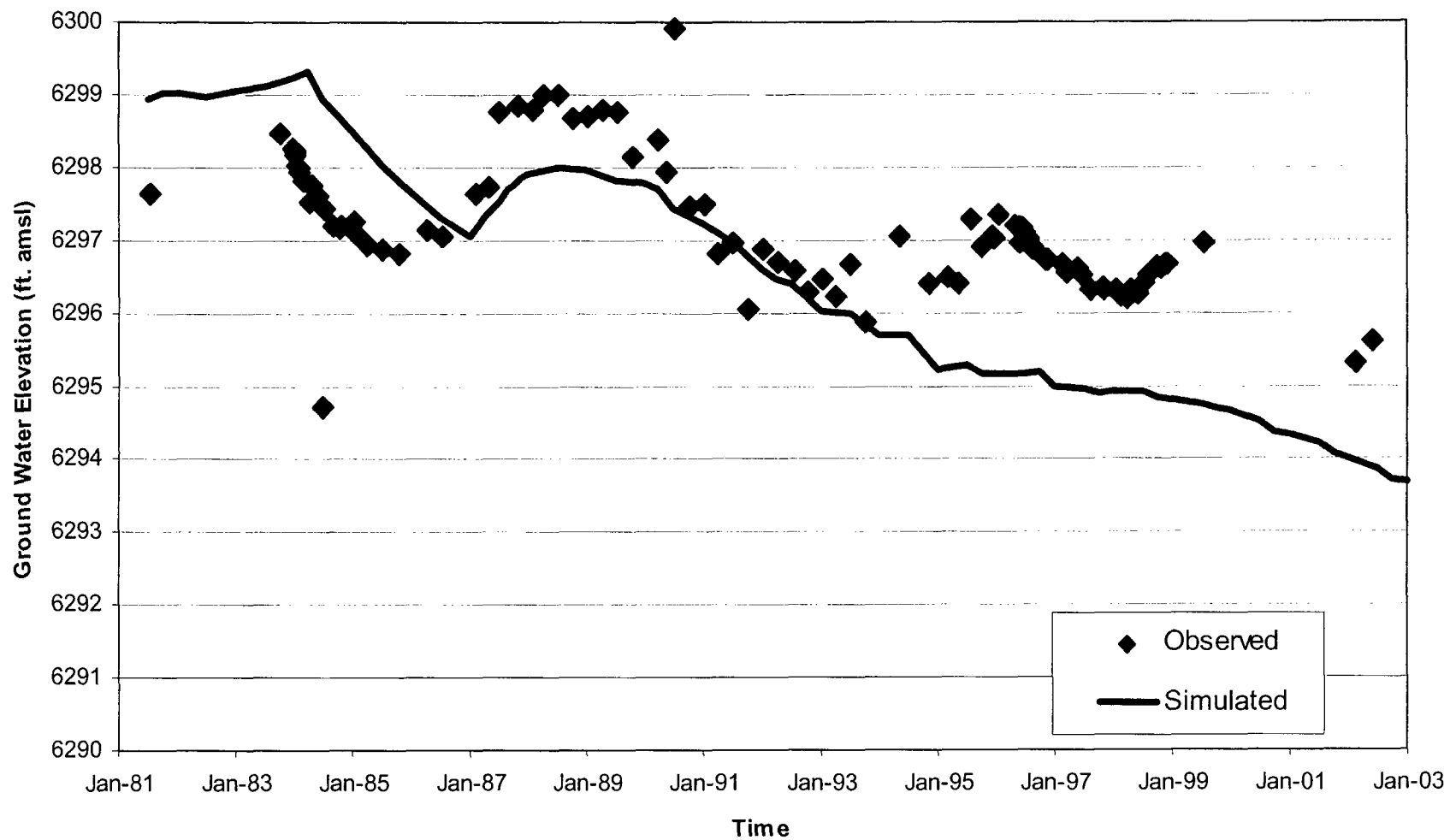


FIGURE 4.6-7
WN-25 OBSERVED vs. SIMULATED
GROUND WATER HYDROGRAPH



consulting
scientists and
engineers

Date: MARCH 2003

Project: P:\03-347\MODEL\REPORT

File: EXCEL-FIGS-4.ppt

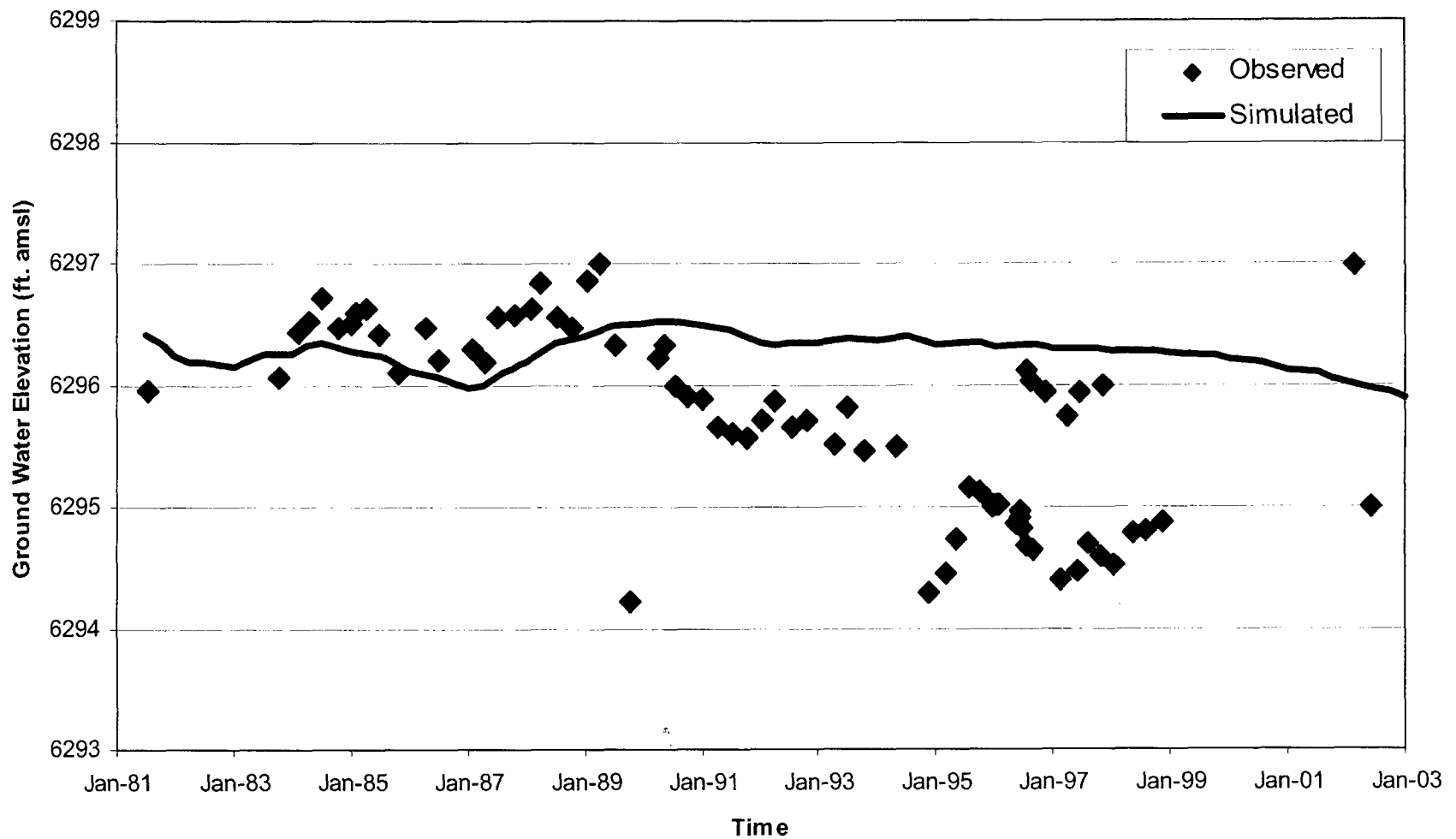


FIGURE 4.6-8
WN-16 OBSERVED vs. SIMULATED
GROUND WATER HYDROGRAPH



consulting
scientists and
engineers

Date: MARCH 2003

Project: P:\03-347\MODEL\REPORT

File: EXCEL-FIGS-4.ppt

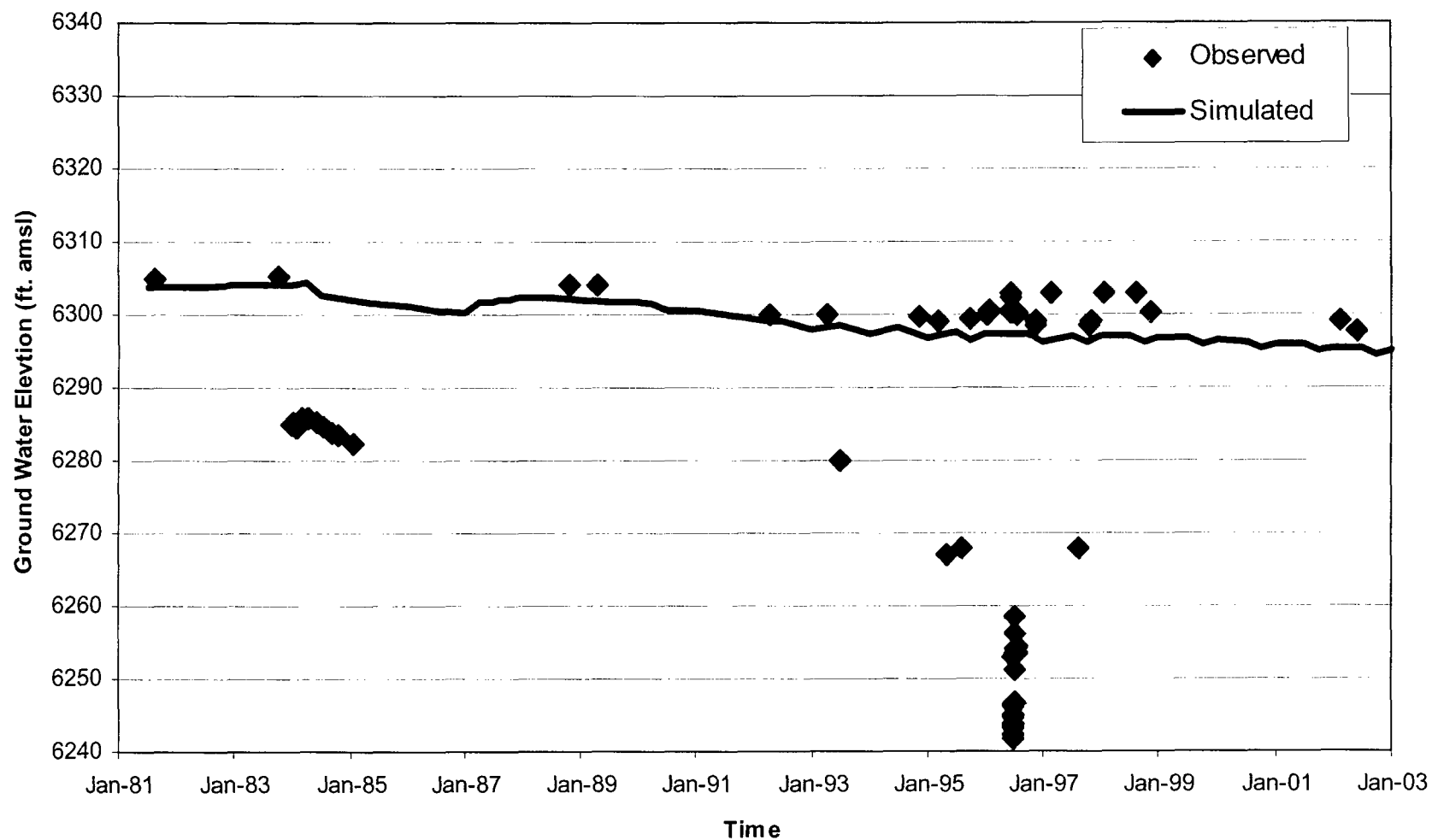


FIGURE 4.6-10
WN-B OBSERVED vs. SIMULATED
GROUND WATER HYDROGRAPH



consulting
scientists and
engineers

Date: MARCH 2003

Project: P:\03-347\MODEL\REPORT

File: EXCEL-FIGS-4.ppt

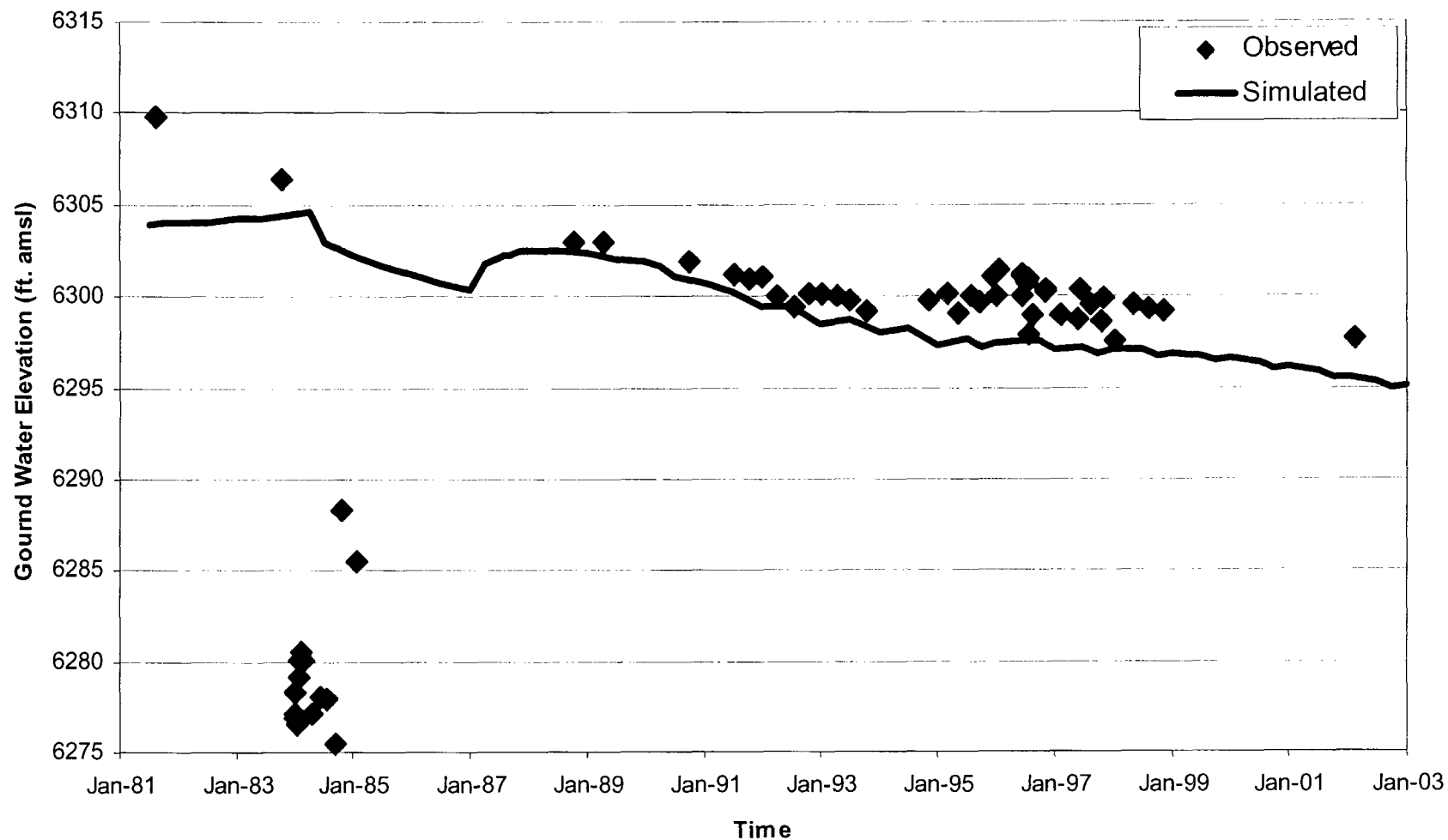


FIGURE 4.6-11
WN-C OBSERVED vs. SIMULATED
GROUND WATER HYDROGRAPH



consulting
scientists and
engineers

Date: MARCH 2003

Project: P:\03-347\MODEL\REPORT

File: EXCEL-FIGS-4.ppt

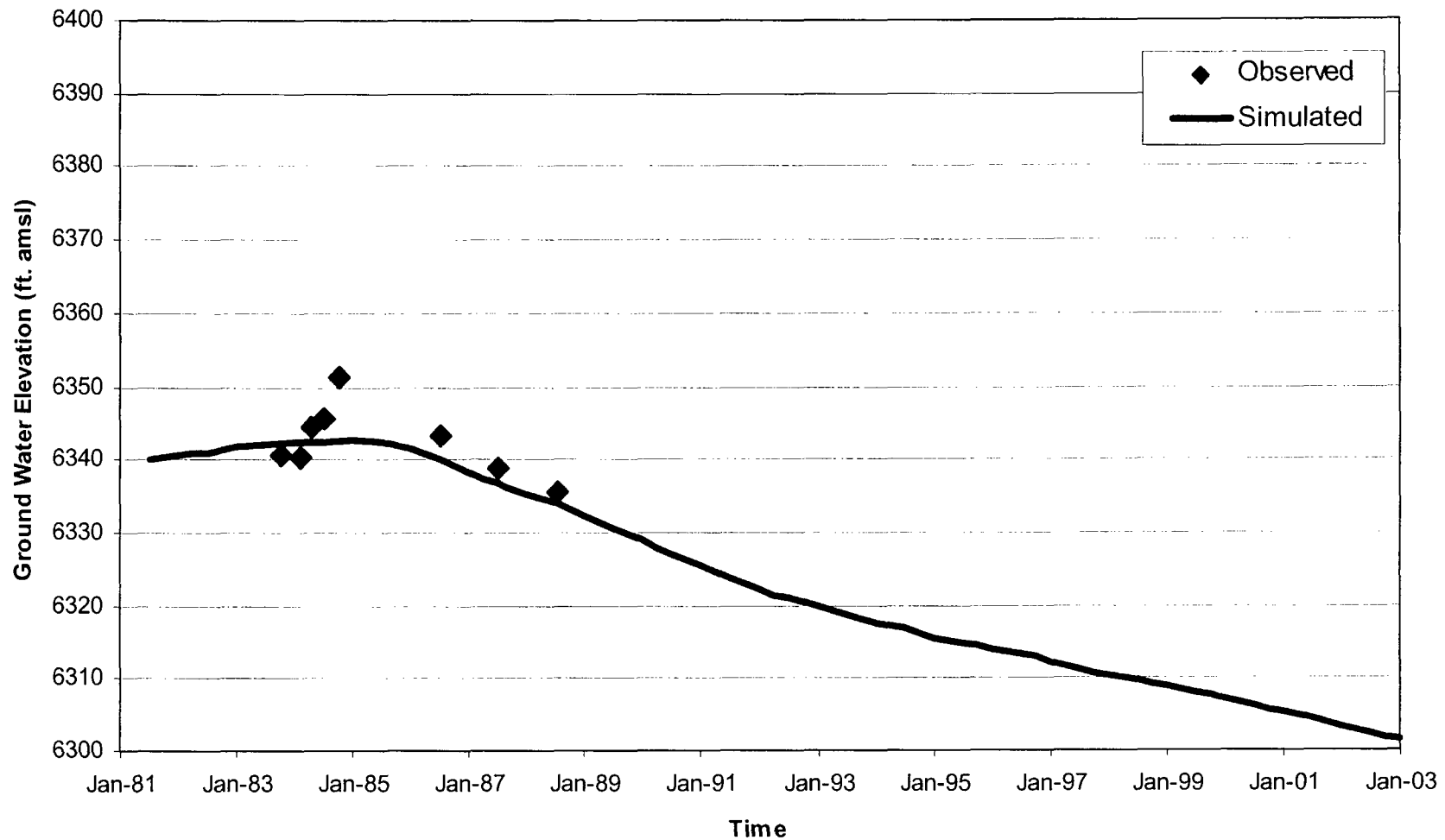


FIGURE 4.6-12
WELL-6 OBSERVED vs. SIMULATED
GROUND WATER HYDROGRAPH



consulting
scientists and
engineers

Date: MARCH 2003

Project: P:\03-347\MODEL\REPORT

File: EXCEL-FIGS-4.ppt

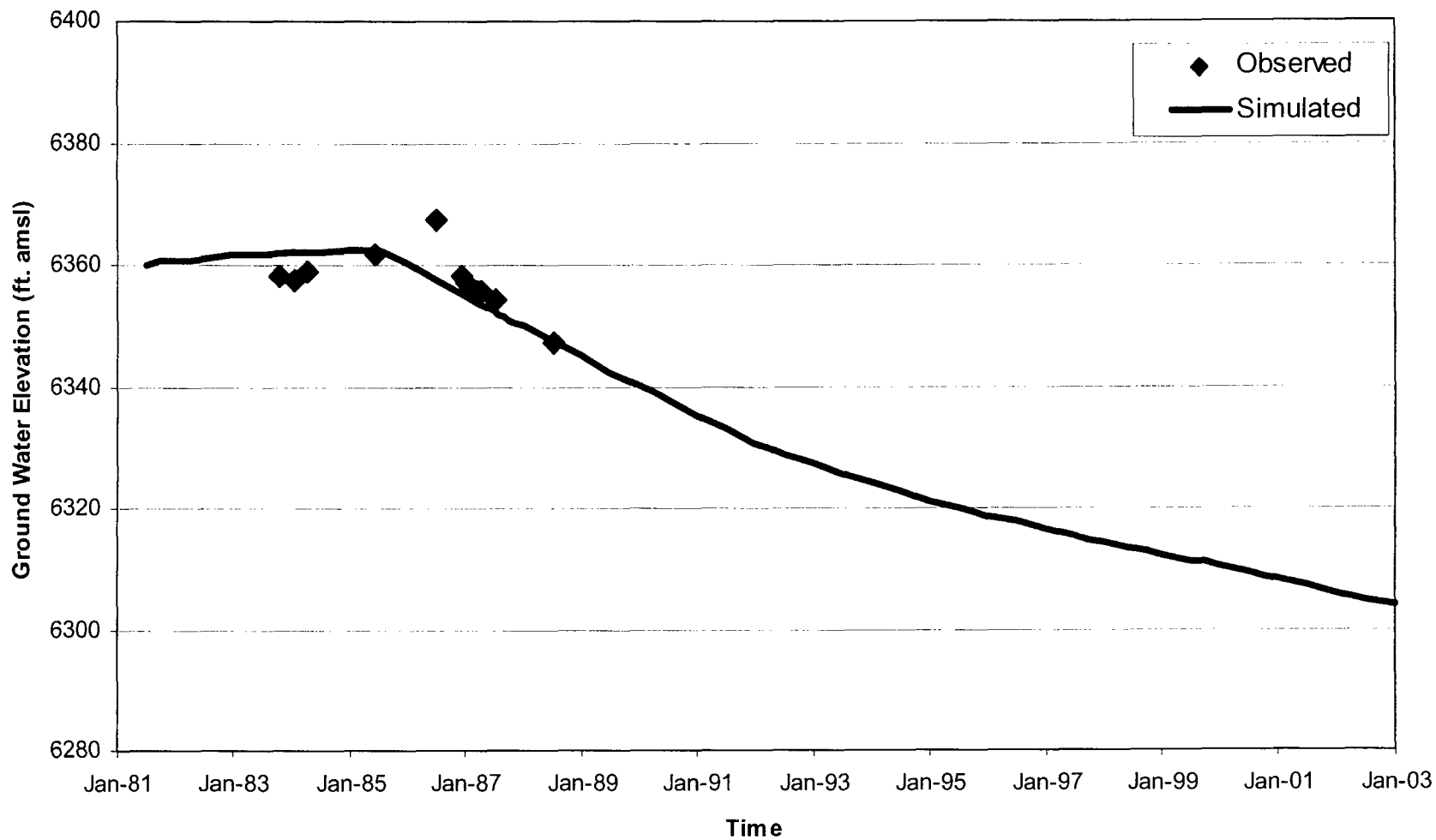


FIGURE 4.6-13
WN-11HT OBSERVED vs. SIMULATED
GROUND WATER HYDROGRAPH



consulting
scientists and
engineers

Date: MARCH 2003

Project: P:\03-347\MODEL\REPORT

File: EXCEL-FIGS-4.ppt

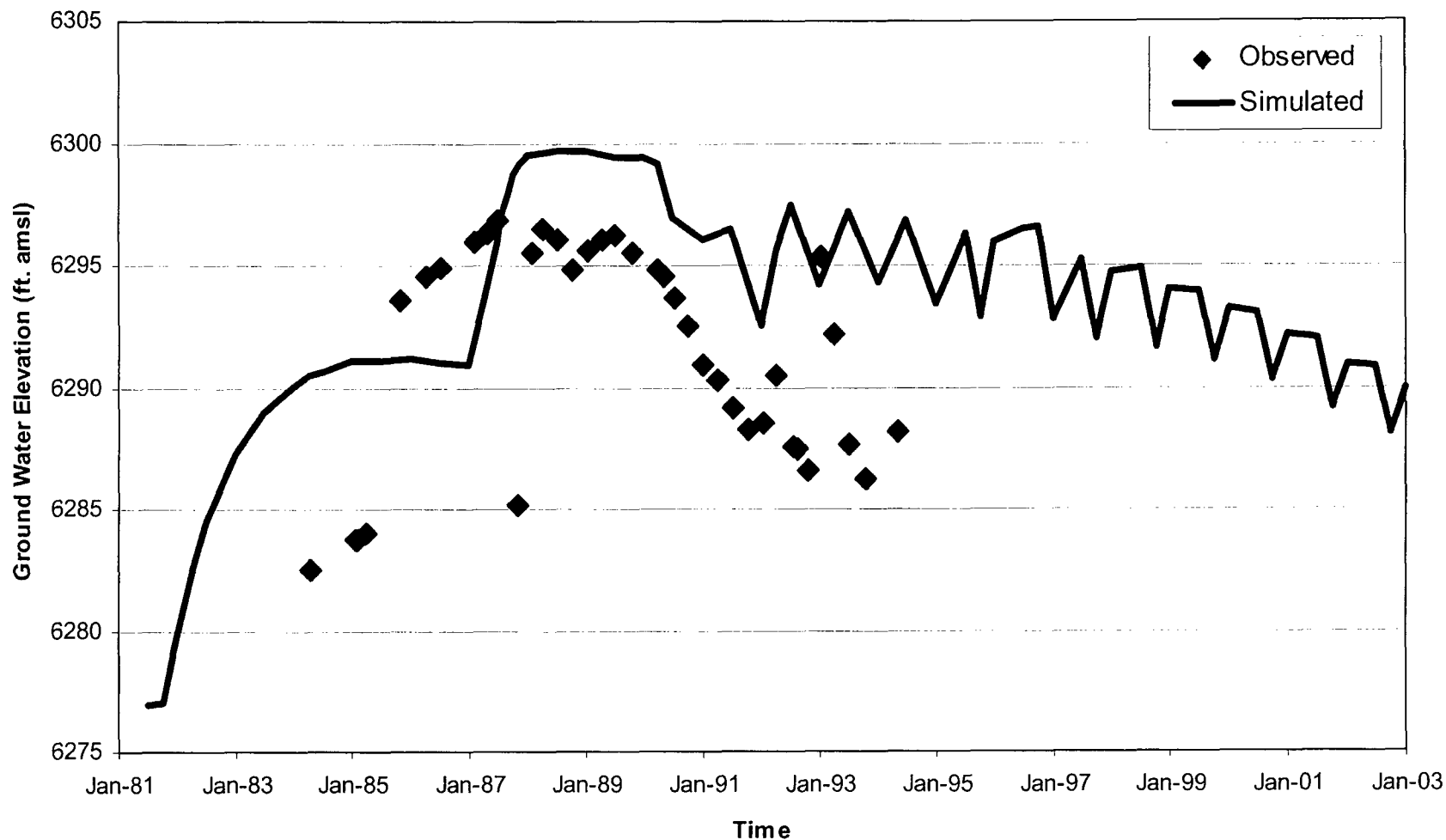


FIGURE 4.6-14
WELL-4 OBSERVED vs. SIMULATED
GROUND WATER HYDROGRAPH



consulting
scientists and
engineers

Date: MARCH 2003

Project: P:\03-347\MODEL\REPORT

File: EXCEL-FIGS-4.ppt

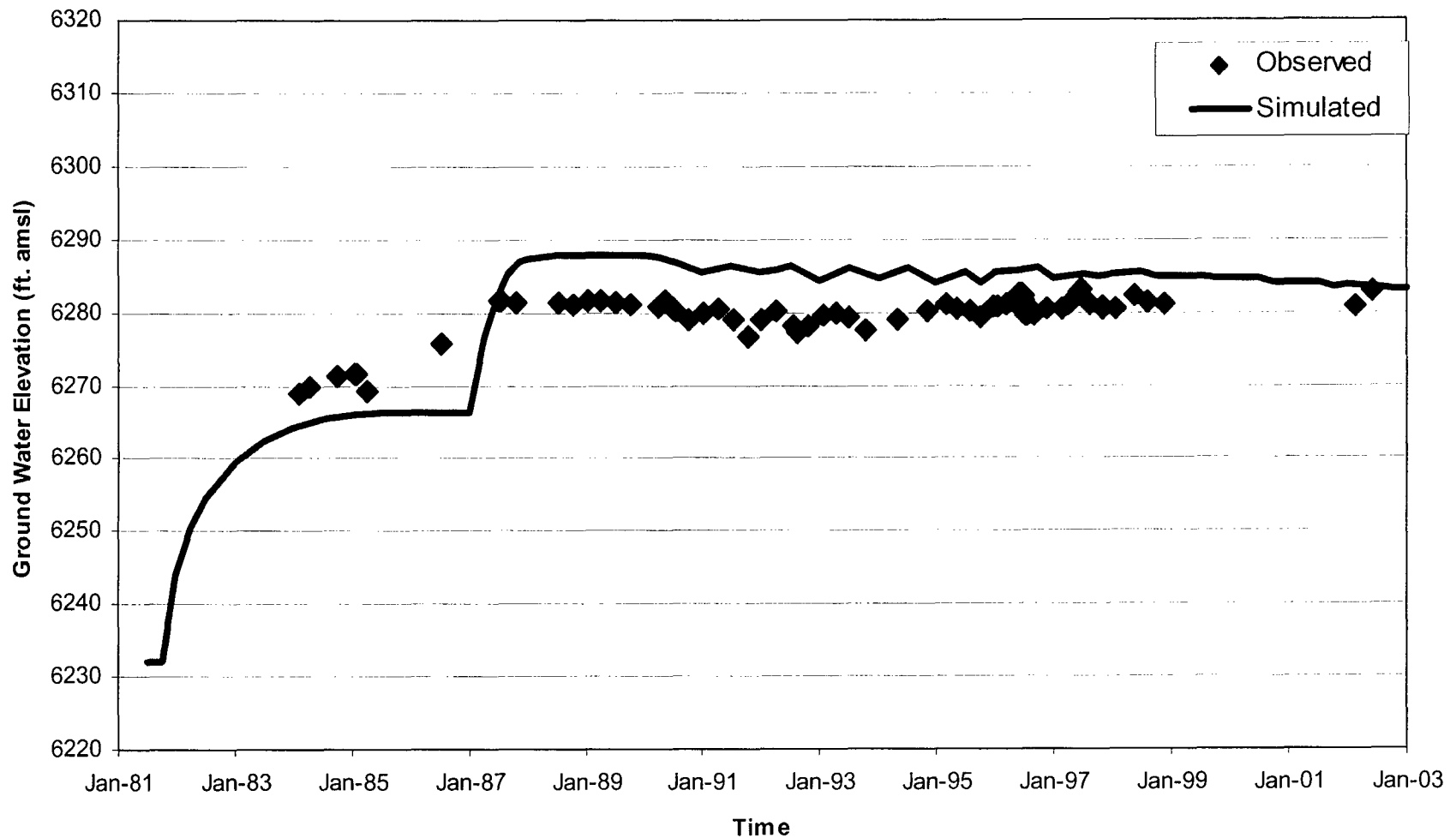


FIGURE 4.6-15
WELL-5 OBSERVED vs. SIMULATED
GROUND WATER HYDROGRAPH



consulting
scientists and
engineers

Date: MARCH 2003

Project: P:\03-347\MODEL\REPORT

File: EXCEL-FIGS-4.ppt

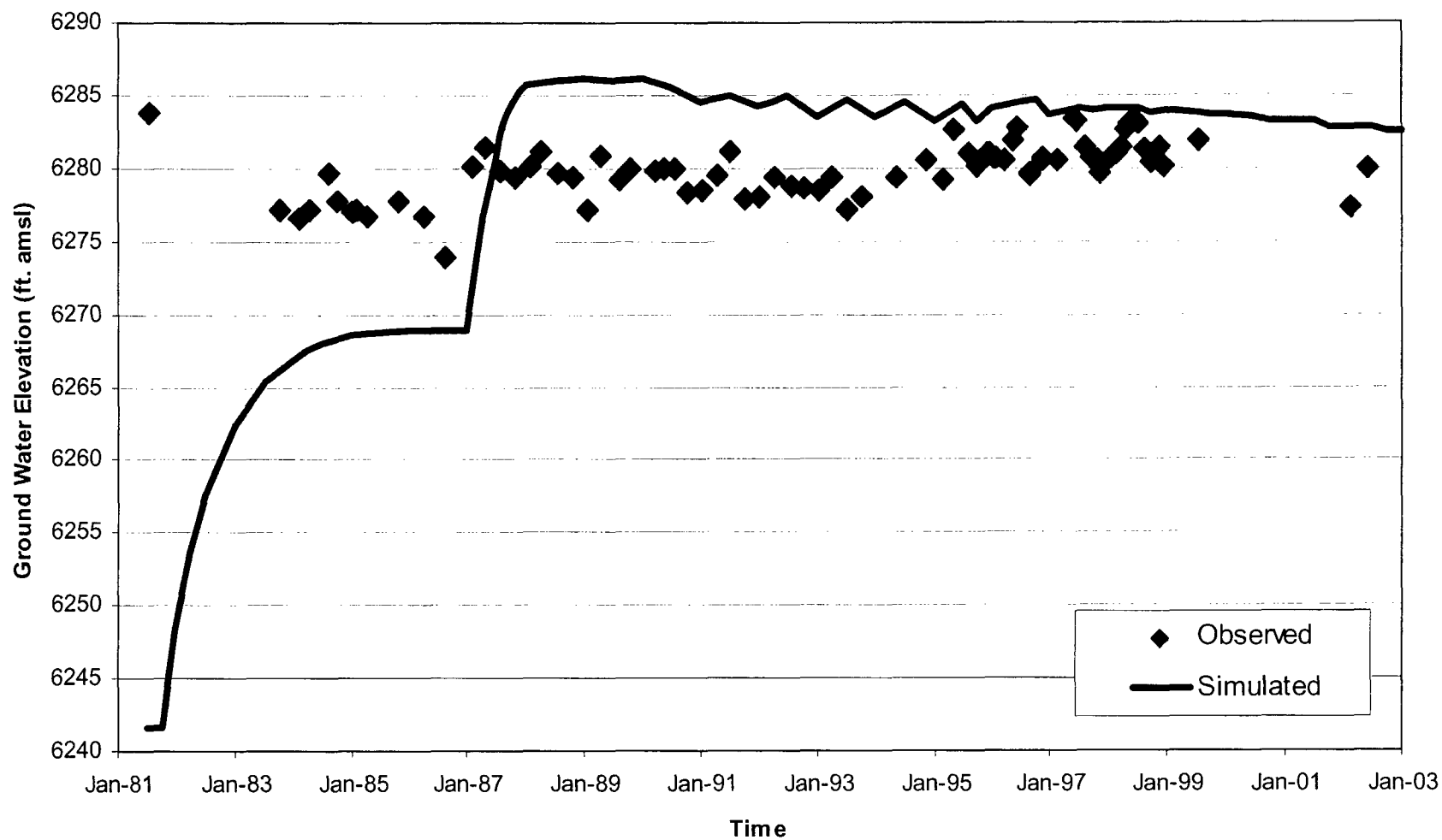


FIGURE 4.6-16
WN-17 OBSERVED vs. SIMULATED
GROUND WATER HYDROGRAPH



consulting
scientists and
engineers

Date: MARCH 2003

Project: P:\03-347\MODEL\REPORT

File: EXCEL-FIGS-4.ppt

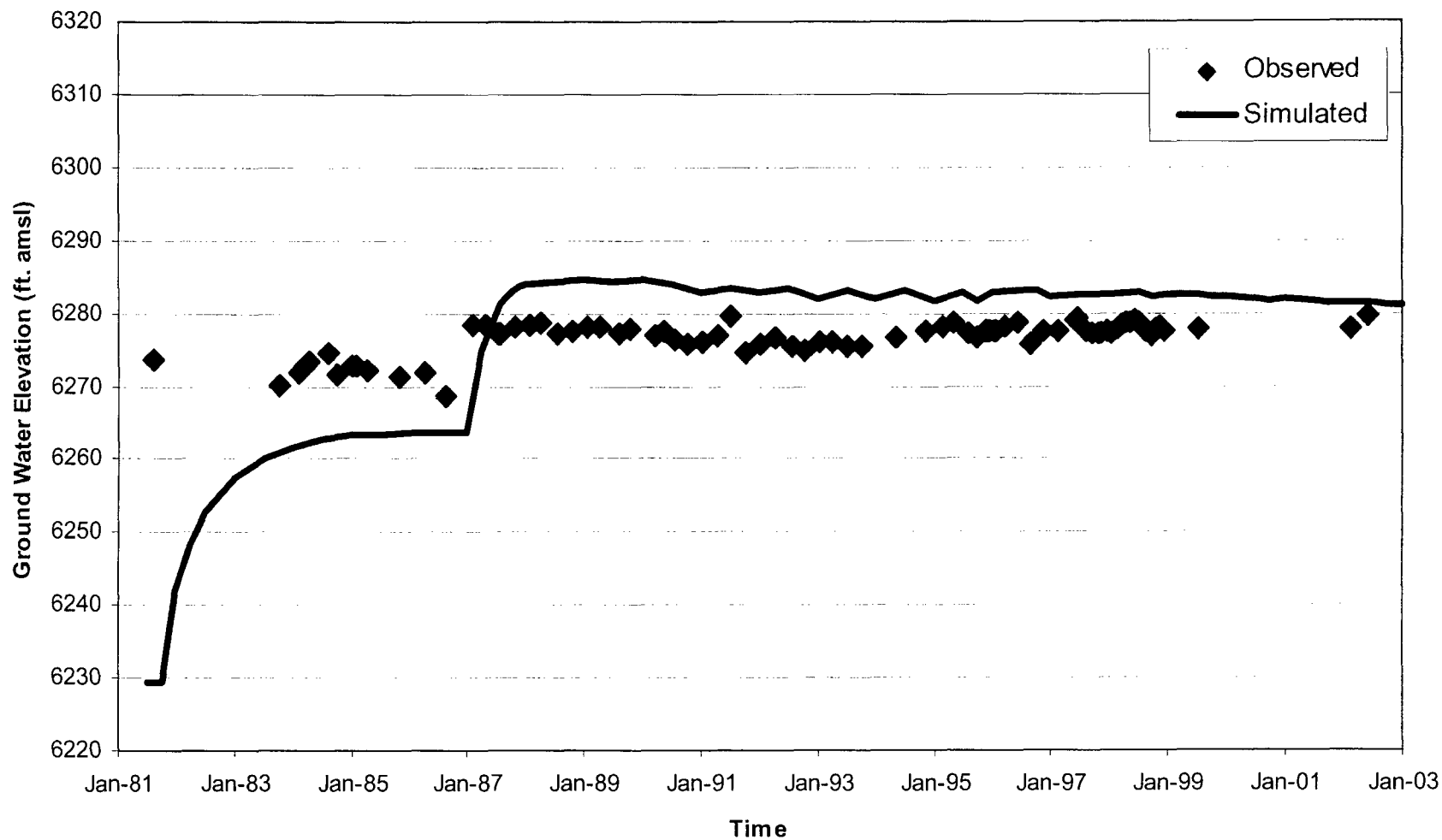


FIGURE 4.6-17
WN-18 OBSERVED vs. SIMULATED
GROUND WATER HYDROGRAPH



consulting
scientists and
engineers

Date: MARCH 2003

Project: P:\03-347\MODEL\REPORT

File: EXCEL-FIGS-4.ppt

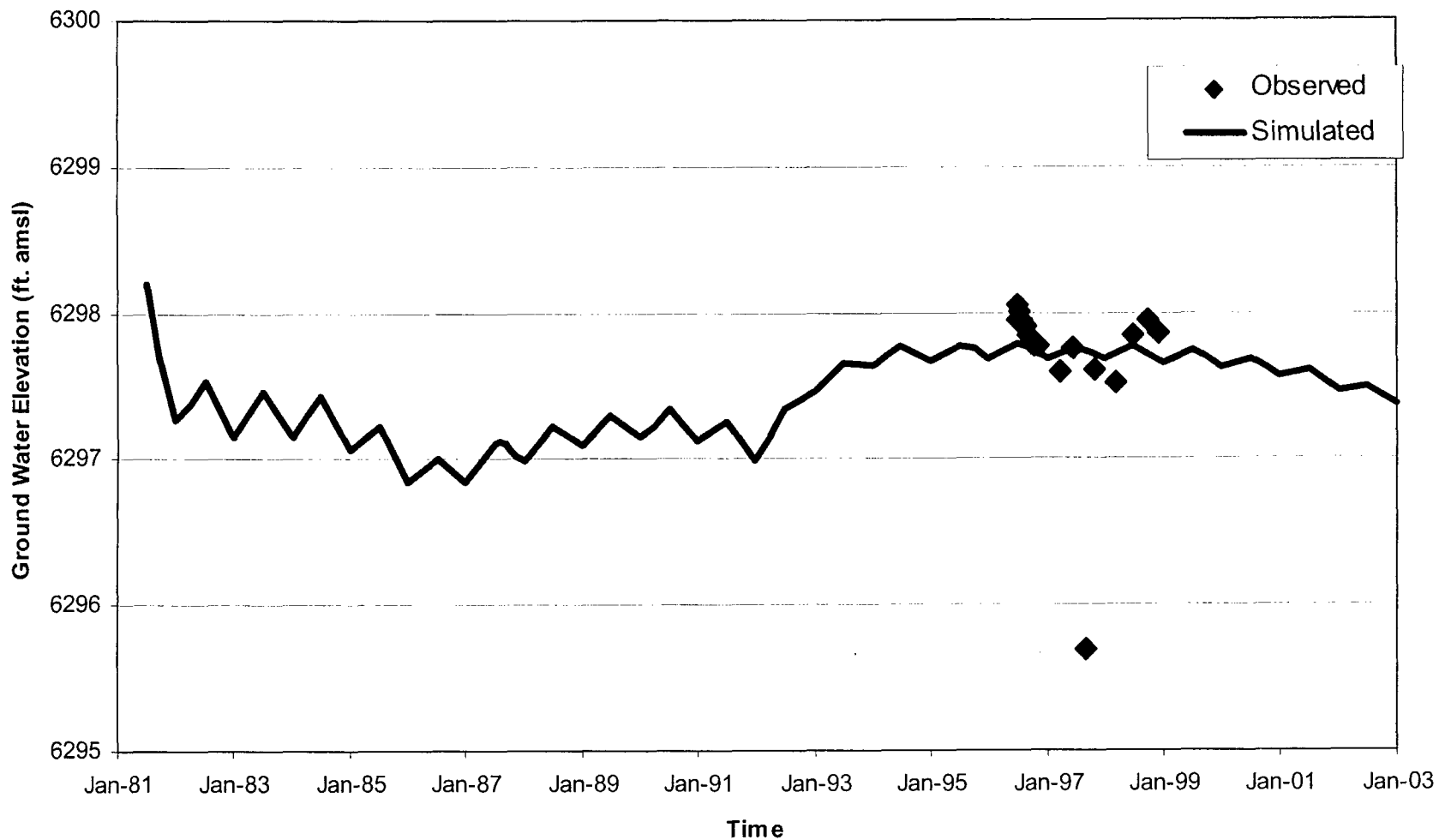


FIGURE 4.6-18
 SWAB-14 OBSERVED vs. SIMULATED
 GROUND WATER HYDROGRAPH



consulting
 scientists and
 engineers

Date: MARCH 2003

Project: P:\03-347\MODEL\REPORT

File: EXCEL-FIGS-4.ppt

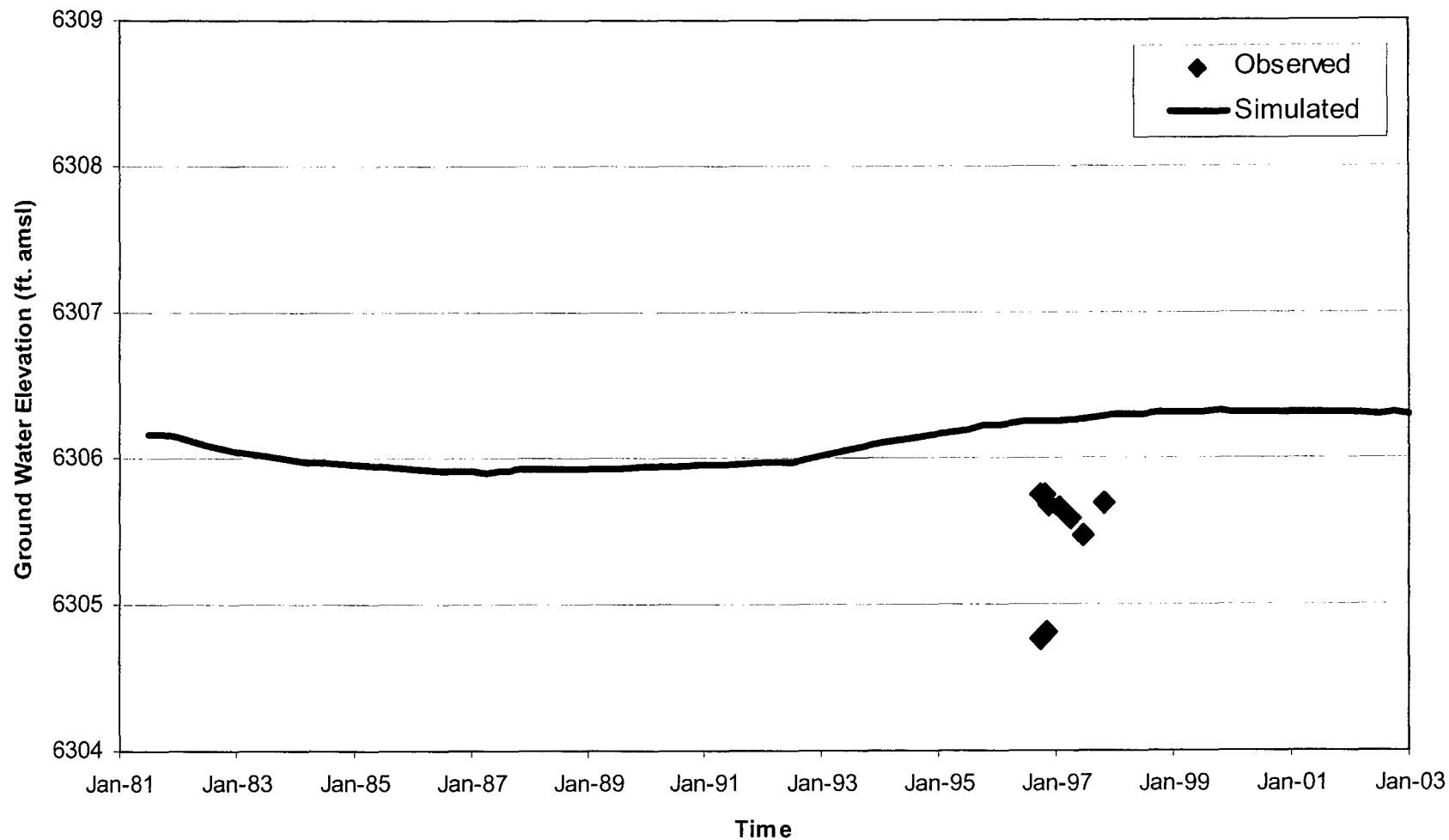


FIGURE 4.6-19
SAB-8 OBSERVED vs. SIMULATED
GROUND WATER HYDROGRAPH



consulting
scientists and
engineers

Date: MARCH 2003

Project: P:\03-347\MODEL\REPORT

File: EXCEL-FIGS-4.ppt

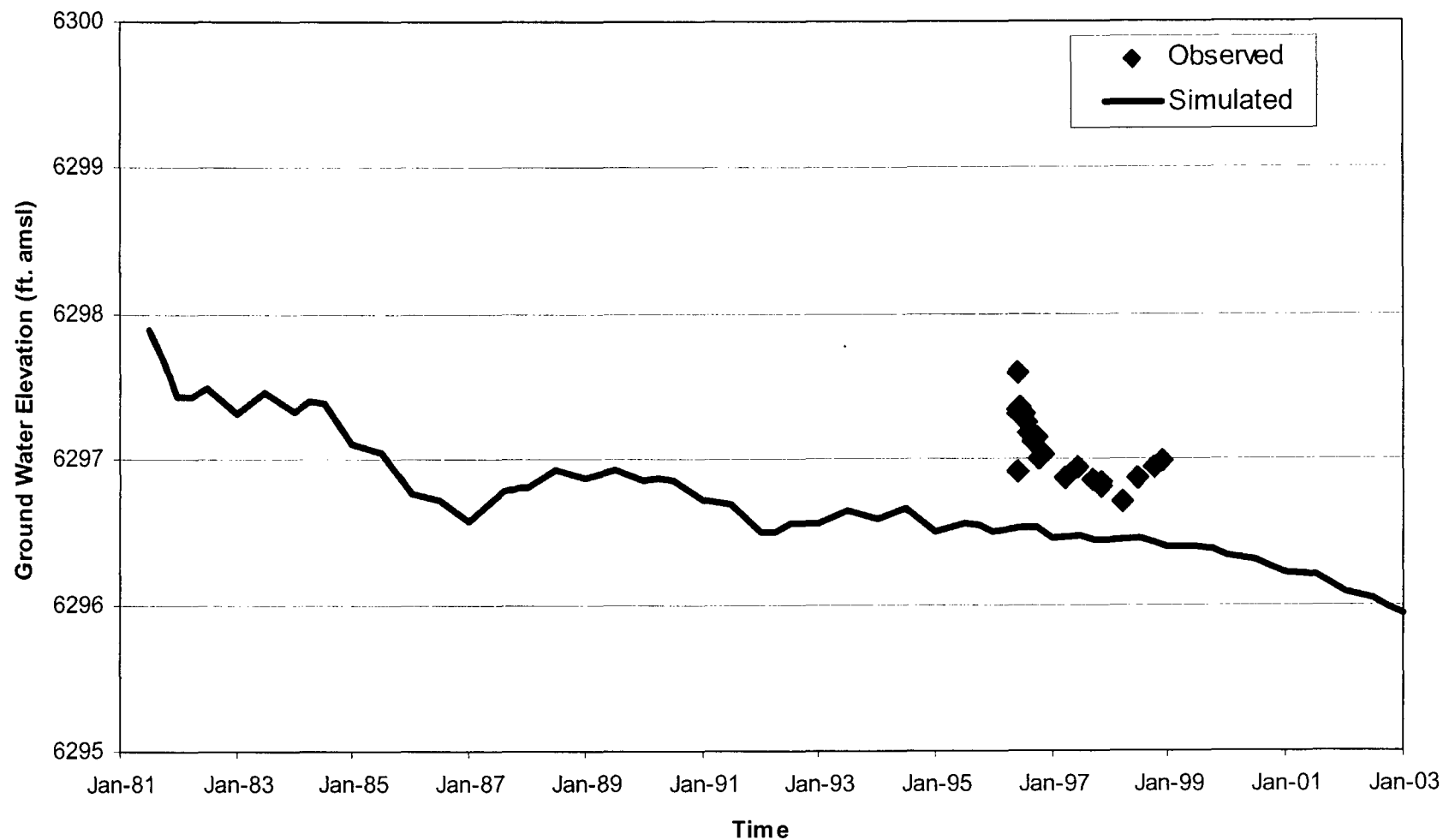


FIGURE 4.6-20
SWAB-6 OBSERVED vs. SIMULATED
GROUND WATER HYDROGRAPH



consulting
scientists and
engineers

Date: MARCH 2003

Project: P:\03-347\MODEL\REPORT

File: EXCEL-FIGS-4.ppt

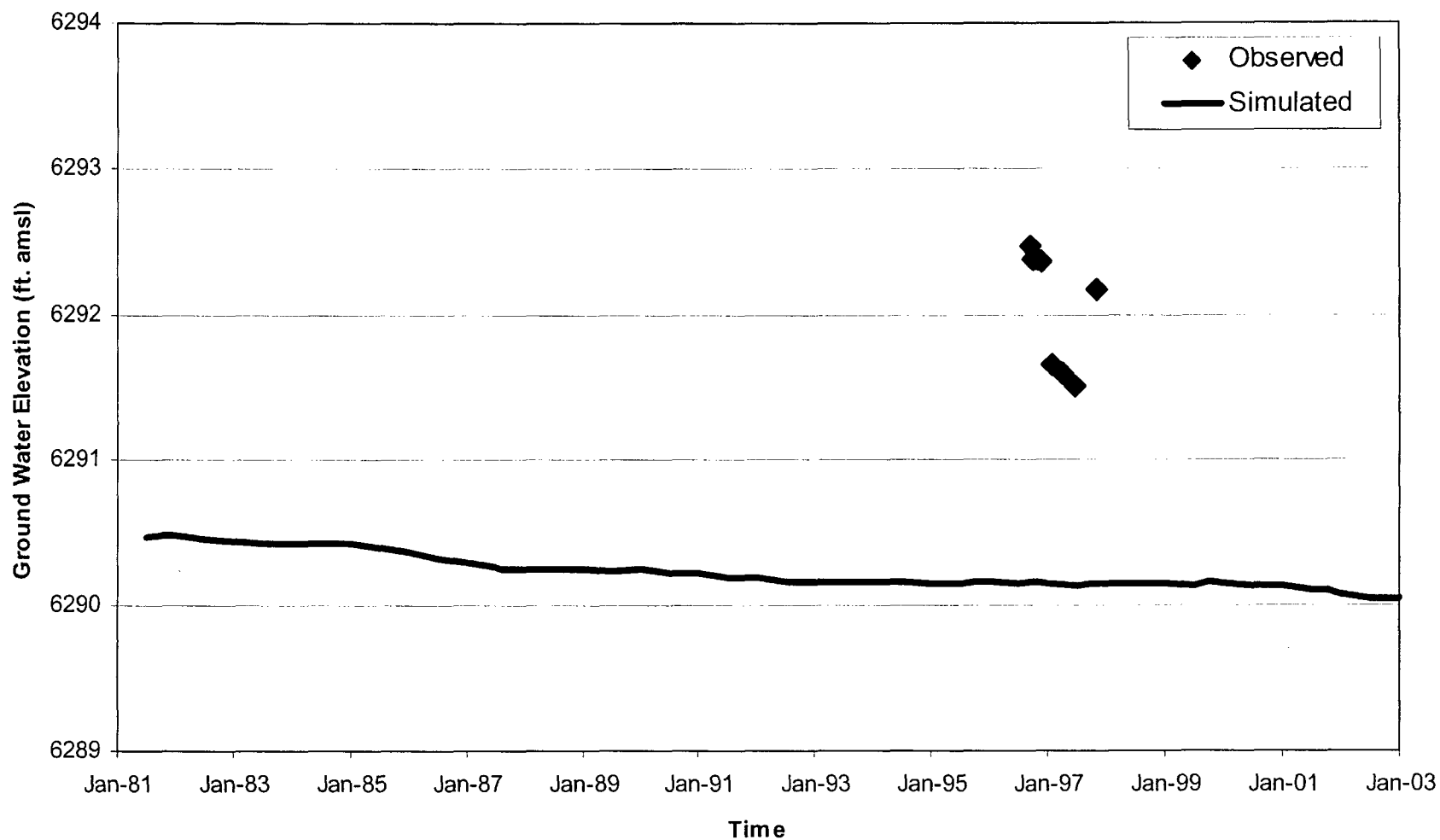


FIGURE 4.6-21
SAB-3 OBSERVED vs. SIMULATED
GROUND WATER HYDROGRAPH



consulting
scientists and
engineers

Date: MARCH 2003

Project: P:\03-347\MODEL\REPORT

File: EXCEL-FIGS-4.ppt

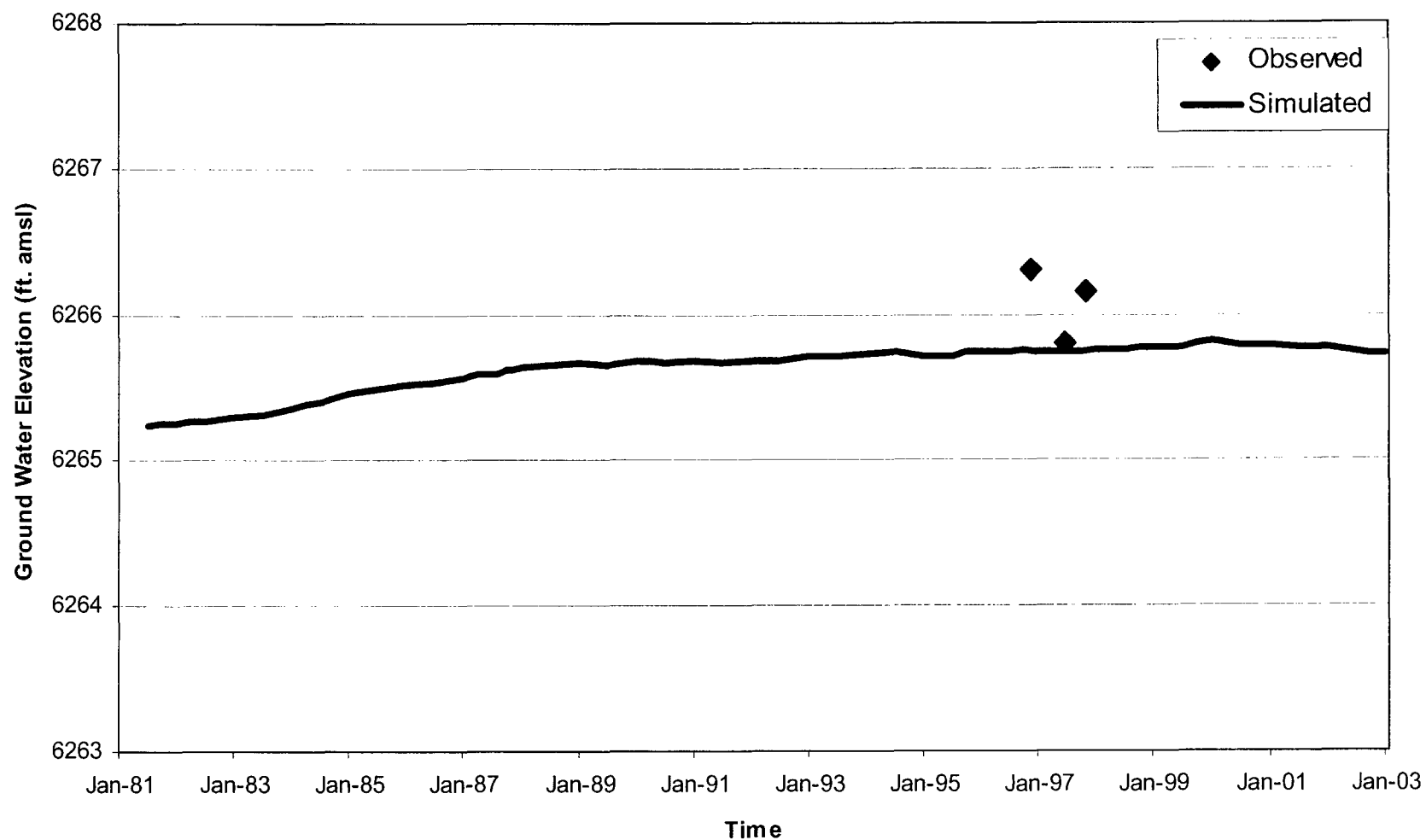


FIGURE 4.6-22
SWAB-33 OBSERVED vs. SIMULATED
GROUND WATER HYDROGRAPH



consulting
scientists and
engineers

Date: MARCH 2003

Project: P:\03-347\MODEL\REPORT

File: EXCEL-FIGS-4.ppt

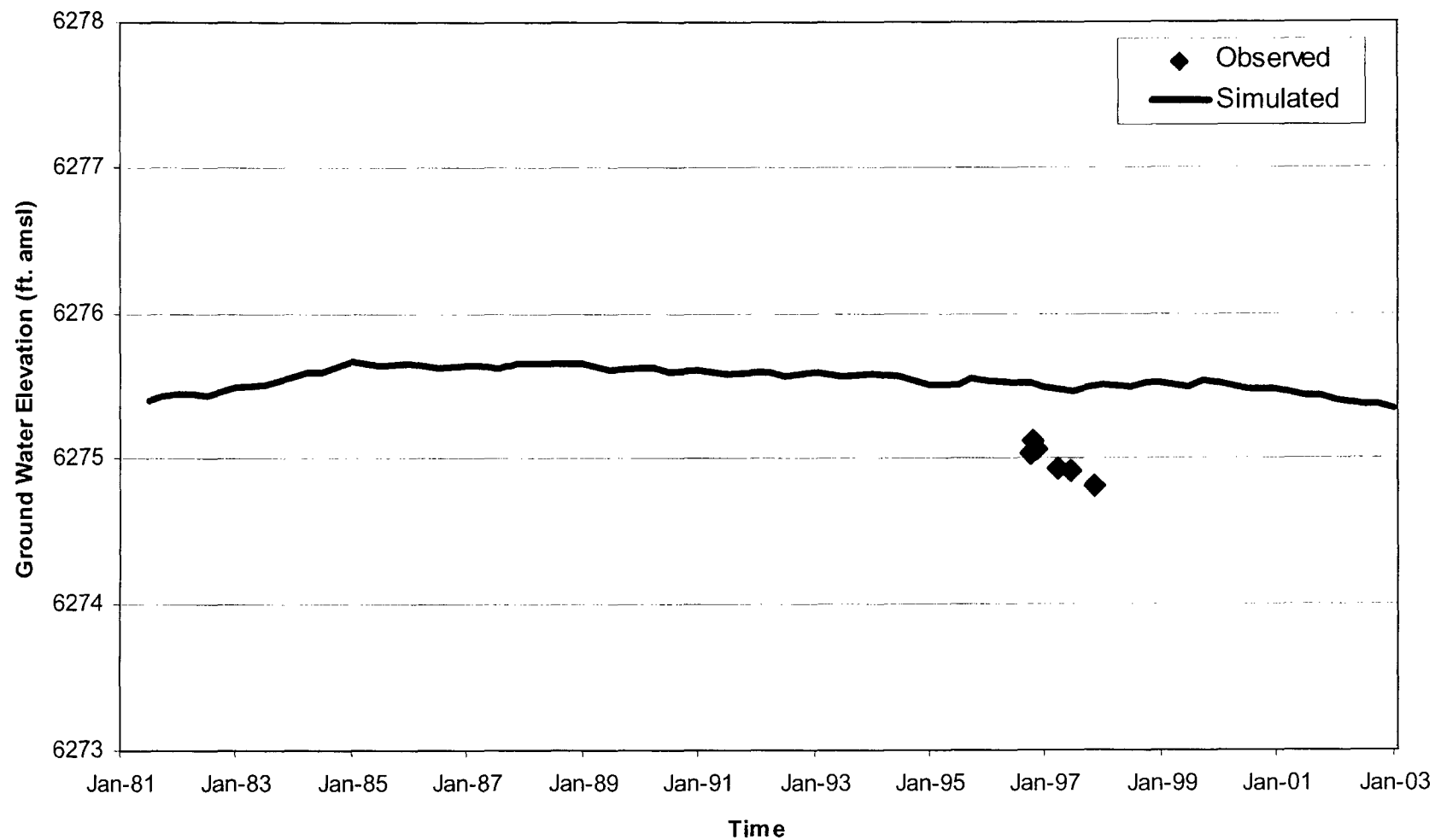


FIGURE 4.6-23
SWAB-31 OBSERVED vs. SIMULATED
GROUND WATER HYDROGRAPH



consulting
scientists and
engineers

Date: MARCH 2003

Project: P:\03-347\MODEL\REPORT

File: EXCEL-FIGS-4.ppt

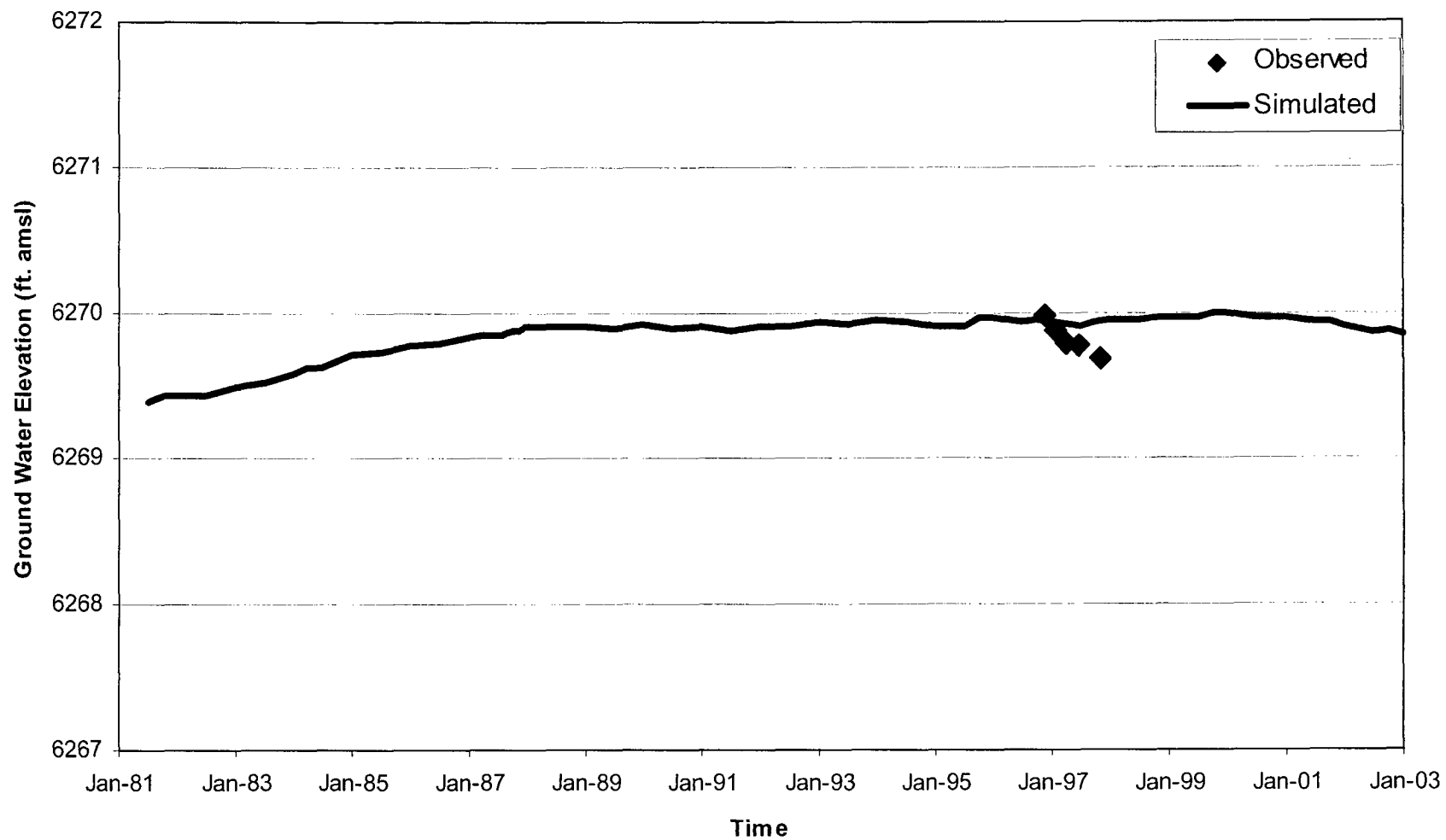


FIGURE 4.6-24
SWAB-34 OBSERVED vs. SIMULATED
GROUND WATER HYDROGRAPH



consulting
scientists and
engineers

Date: MARCH 2003

Project: P:\03-347\MODEL\REPORT

File: EXCEL-FIGS-4.ppt

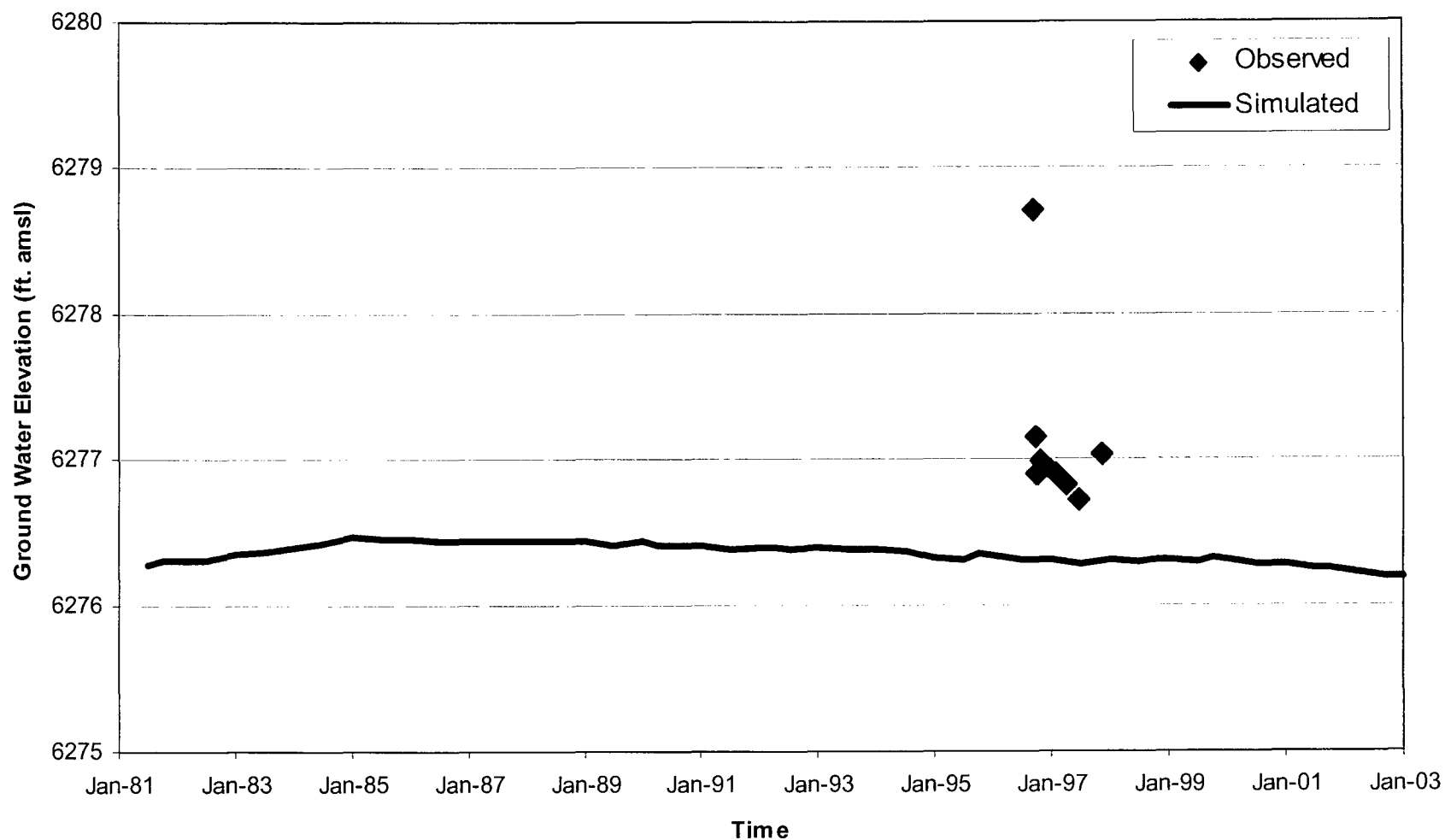


FIGURE 4.6-25
SWAB-32 OBSERVED vs. SIMULATED
GROUND WATER HYDROGRAPH



consulting
scientists and
engineers

Date: MARCH 2003

Project: P:\03-347\MODEL\REPORT

File: EXCEL-FIGS-4.ppt

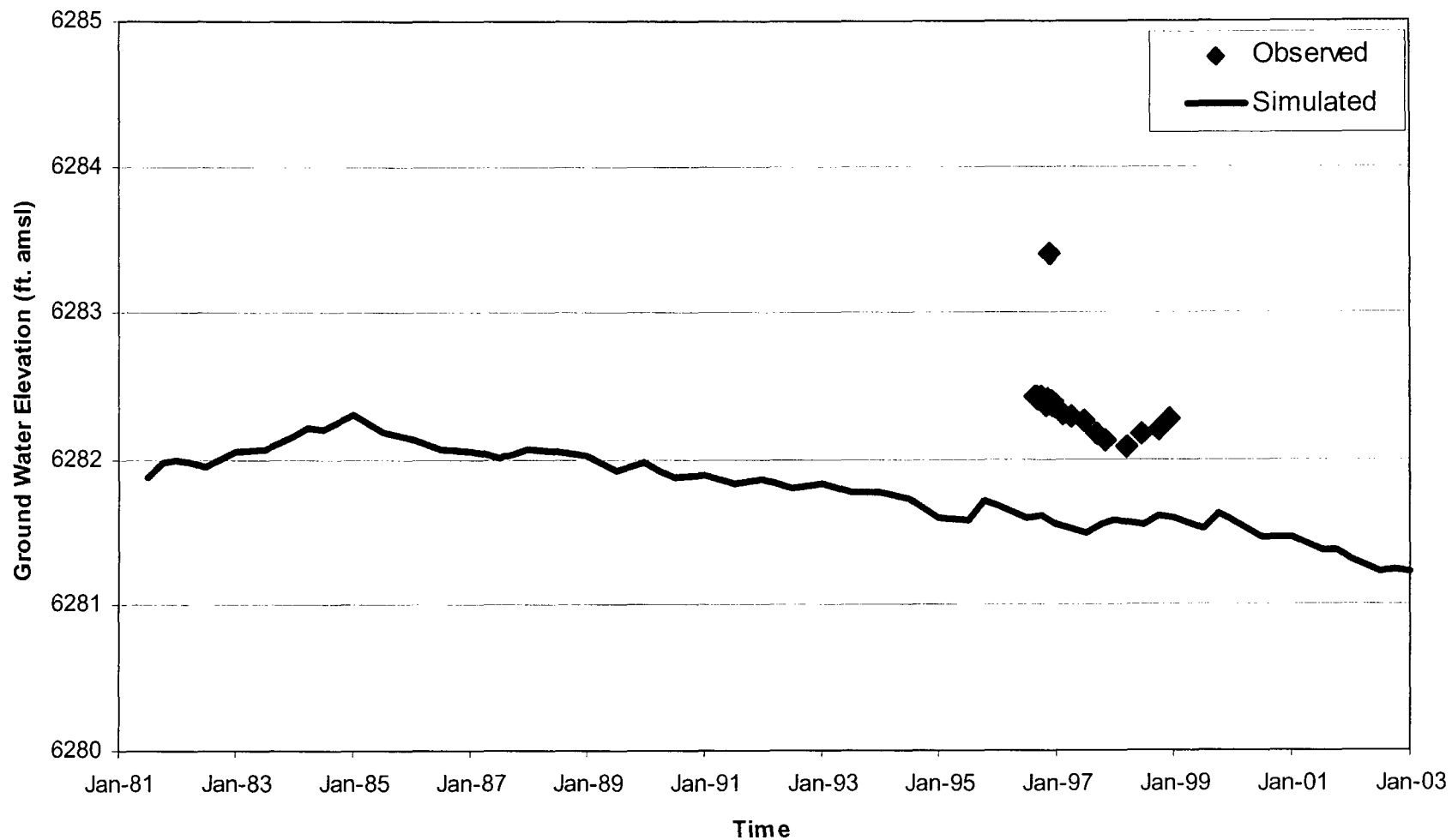


FIGURE 4.6-26
 SWAB-29 OBSERVED vs. SIMULATED
 GROUND WATER HYDROGRAPH



consulting
 scientists and
 engineers

Date: MARCH 2003

Project: P:\03-347\MODEL\REPORT

File: EXCEL-FIGS-4.ppt